

Phosphatidylserine phospholipase A1 enables GPR34-dependent immune cell accumulation in the peritoneal cavity

by  
Hanson Tam

DISSERTATION

Submitted in partial satisfaction of the requirements for degree of  
DOCTOR OF PHILOSOPHY

in

Biomedical Sciences

in the

GRADUATE DIVISION

of the

UNIVERSITY OF CALIFORNIA, SAN FRANCISCO

Approved:

DocuSigned by:

*Matthew Spitzer*

Matthew Spitzer

4793AE6232BE479...

Chair

DocuSigned by:

*Jason Cyster*

Jason Cyster

DocuSigned by:

*Clifford Lowell*

Clifford Lowell

1EA1A95C4F734C7...

---

Committee Members



To my parents, Lily Tam and Donald Tam,  
for their endless love and support

## ACKNOWLEDGEMENTS

I am grateful to the many people who made this work possible. First and foremost, I would like to thank my PhD advisor Dr. Jason Cyster. I joined Jason's lab because of his rigorous, mechanistic approach to dissecting problems and his unparalleled dedication to trainees. For these reasons, Jason's mentorship has been transformative for my growth as a scientist. Through our weekly meetings, I have learned to design well-controlled experiments and to critically analyze data. Jason's incisive capacity for positioning results in the context of published literature has shaped my ability to see the bigger picture. At the same time, he has taught me to guard against biases with his recurrent reminder that science is about failing to disprove, rather than seeking to prove. I have also benefitted from Jason's seemingly limitless availability to support me despite his busy schedule. There have been countless occasions where Jason made time to meet on short notice to review data, to provide feedback on my writing, or to allow me to practice a presentation. When my projects hit roadblocks, he put in extra effort to troubleshoot and brainstorm new approaches with me. In addition to supporting me scientifically, Jason has consistently supported my career and personal goals. I am very grateful to have Jason as my PhD mentor.

Thank you to my thesis committee members, Dr. Matthew Spitzer and Dr. Clifford Lowell, for providing constructive feedback and perspective on my work, for generously sharing their lab resources and expertise, and for offering helpful professional advice. Thank you also to Dr. Clifford Lowell, Dr. Lewis Lanier, Dr. Adrian Erlebacher, and Dr. Mehrdad Matloubian, for critically evaluating my scientific thinking as members of my qualifying exam committee, and to Dr. Averil Ma, for support and advice as my MSTP and BMS advisor. I am additionally thankful

to my rotation mentor, Dr. Michael Rosenblum, as well as Dr. Jarish Cohen in the Rosenblum lab from whom I first learned to work with mice.

I would like to acknowledge several scientific mentors who shaped my decision to pursue a PhD. My first exposure to research was through my high school biology teacher, Dr. Christina Weaver, who instilled in me the importance of good record keeping and who connected me with Dr. Betsy Mellins at Stanford. In the Mellins lab, I worked directly with Dr. Claudia Macaubas, who taught me the fundamentals of wet lab research. Under the patient and dedicated mentorship of Claudia and Betsy, I fell in love with scientific discovery. As a pediatric rheumatologist studying her patients' autoimmune diseases, Betsy also played an early role in inspiring me to pursue a physician-scientist career path. During my undergraduate studies, I worked with Dr. Jimmy Martenson in Dr. Vladimir Denic's lab. Jimmy and Vlad reinforced my growing interest in mechanism, trained me in the basics of experimental design, and taught me how to be an independent and resilient scientist.

During my time in the Cyster lab, I have been fortunate to work with extraordinary colleagues. Dr. Marco De Giovanni was a fantastic rotation mentor, walking me through every detail and answering my numerous questions. Marco generously shared his technical expertise and deep knowledge of immunology. Dr. Elise Wolf and Dr. Marissa Chou were my first baymates and taught me everything from reagent locations to how to thrive in the lab. Their advice and friendship made me feel welcome and supported. As a senior MSTP student, Marissa has also been an invaluable resource and mentor, helping me navigate the MD-PhD program. Thank you to the many talented post-docs who have shown me techniques and who have provided helpful discussions, feedback, and advice: Dr. Dan Liu, Dr. Ben Winer, Dr. Finn Wolfreys, Dr. Lihui Duan, Dr. Jianxuan Wu, Dr. Adi Biram, Dr. Tamar Ben-Shaanan, Dr. Jessica

Kotov, Dr. Konrad Knöpper, Dr. Zachary Earley, Dr. Taylor LaFlam, Dr. Hannah Huang, Dr. Fanglue Peng, Dr. Jianhang Yin, and Dr. Norihide Jo. Thank you to my fellow graduate students—Kevin Chen, Nikhita Kirthivasan, Charles Shen, and Lexi Schneider—for making the lab a lively place to do science and for sharing in the ups and downs of graduate school. I am grateful to Jinping An and Ying Xu for crucial assistance with the mouse colony, genotyping, and molecular biology. Thank you to Hanna Taglinao and Anshul Rao for organizing the lab, to Viviana Davila and Annie Yee for handling lab operations, and to Bernarda Lopez for keeping everything stocked and running smoothly. Thank you to the LARC staff, especially Karla Mendoza, for caring for our mice.

I would also like to express my appreciation to the directors and administrators of the MSTP and BMS program for their guidance and support: Dr. Mark Anderson, Dr. Aimee Kao, Dr. Mark Ansel, Dr. Anita Sil, Dr. Adrian Erlebacher, Geri Ehle, Dr. Tiffani Quan, Demian Sainz, Meridith Miner, Andrés Zepeda, Brianne Bustamente, Marcelo Pereira, Vivian Parker, and Amanda Andonian.

Thank you to my partner, Jacquelyn Ho, for being my closest confidante and best friend. Thank you for always believing in me, for bringing balance to my life, and for lighting up my world. Your love keeps me going every day.

Finally, thank you to my family. My sister, Tiffany Tam, has kept me grounded and reminds me of the things that are most important in life. And to my parents—thank you for your unwavering love and support in all my endeavors and for all the sacrifices you have made for my happiness and wellbeing.

## CONTRIBUTIONS TO PRESENTED WORK

All work presented in this dissertation was performed under the direct supervision and guidance of Dr. Jason G. Cyster. Chapter 2 is adapted from a manuscript published in *Journal of Experimental Medicine*, “Phosphatidylserine phospholipase A1 enables GPR34-dependent immune cell accumulation in the peritoneal cavity.” The thesis abstract was adapted from this work. The co-authors for this publication were Ying Xu, Jinping An, Torsten Schöneberg, Angela Schulz, Jagan R. Muppidi, and Jason G. Cyster. Jason G. Cyster and I conceptualized the study, designed the experiments, analyzed the data, and wrote the manuscript. I performed most experiments. Ying Xu cloned retroviral constructs, prepared the RNA sequencing library, and performed qPCR. Ying Xu and Jinping An genotyped mice. Torsten Schöneberg and Angela Schulz contributed *Gpr34<sup>KO</sup>* mice and provided input on the manuscript. Jagan R. Muppidi performed informative preliminary experiments, contributed helpful discussion, and provided input on the manuscript.

**Phosphatidylserine phospholipase A1 enables GPR34-dependent immune cell accumulation  
in the peritoneal cavity**

Hanson Tam

**ABSTRACT**

The peritoneal cavity (PerC) is an important site for immune responses to infection and cancer metastasis. Yet few ligand–receptor axes are known to preferentially govern immune cell accumulation in this compartment. GPR34 is a lysophosphatidylserine (lysoPS)-responsive receptor that frequently harbors gain-of-function mutations in mucosa-associated B cell lymphoma. Here, we set out to test the impact of a GPR34 knock-in (KI) allele in the B-lineage. We report that GPR34 KI promotes the PerC accumulation of plasma cells (PC) and memory B cells (MemB). These KI cells migrate robustly to lysoPS *ex vivo*, and the KI allele synergizes with a Bcl2 transgene to promote MemB but not PC accumulation. Gene expression and labeling studies reveal that GPR34 KI enhances PerC MemB proliferation. Both KI PC and MemB are specifically enriched at the omentum, a visceral adipose tissue containing fibroblasts that express the lysoPS-generating PLA1A enzyme. Adoptive transfer and chimera experiments revealed that KI PC and MemB maintenance in the PerC is dependent on stromal PLA1A. These findings provide *in vivo* evidence that PLA1A produces lysoPS that can regulate GPR34-mediated immune cell accumulation at the omentum.

## TABLE OF CONTENTS

<b>CHAPTER 1: Introduction</b> .....	<b>1</b>
<b>Peritoneal cavity immunity</b> .....	<b>2</b>
<b>GPR34 is a lysophosphatidylserine receptor</b> .....	<b>5</b>
<b>Functions of GPR34 in immune cells</b> .....	<b>8</b>
<b>CHAPTER 2: Phosphatidylserine phospholipase A1 enables GPR34-dependent immune cell accumulation in the peritoneal cavity</b> .....	<b>11</b>
<b>ABSTRACT</b> .....	<b>12</b>
<b>INTRODUCTION</b> .....	<b>13</b>
<b>RESULTS AND DISCUSSION</b> .....	<b>16</b>
Generation of GPR34 GOF KI mice.....	16
GPR34 KI promotes the PerC accumulation of PC and MemB .....	19
PC and B cell abundance are unaltered in GPR34-deficient mice.....	21
GPR34 KI cells migrate to lysoPS ex vivo .....	22
Conditional activation of GPR34 KI is sufficient for PerC PC accumulation .....	22
KI PerC MemB accumulation is enhanced by Bcl2 overexpression .....	25
GPR34 KI enhances MemB proliferation.....	26
The omentum is enriched for KI PC and MemB .....	26
Stromal PLA1A is required for PerC KI PC and MemB maintenance.....	31
Concluding remarks .....	35
<b>SUPPLEMENTARY FIGURES</b> .....	<b>38</b>
<b>MATERIALS AND METHODS</b> .....	<b>44</b>
Mice .....	44

Treatments and immunizations .....	45
Cell preparation.....	45
Adoptive transfer experiments .....	46
Flow cytometry .....	47
Cell sorting and RNA sequencing.....	48
Published scRNAseq data analysis .....	49
Generation of GPR34-expressing WEHI-231 cells .....	49
Transwell migration assays .....	49
Immunofluorescence staining and microscopy.....	50
LC-MS/MS .....	50
Quantitative PCR .....	51
Statistical analyses .....	52
<b>DATA AVAILABILITY .....</b>	<b>53</b>
<b>ACKNOWLEDGEMENTS .....</b>	<b>53</b>
<b>CHAPTER 3: Conclusion.....</b>	<b>54</b>
<b>Conclusion .....</b>	<b>55</b>
<b>REFERENCES.....</b>	<b>59</b>

## LIST OF FIGURES

### CHAPTER 1: Introduction

Figure 1.1. Schematic of the mouse peritoneal cavity. ....	2
Figure 1.2 GPR34 is a G <sub>i</sub> -coupled lysophosphatidylserine receptor. ....	5
Figure 1.3. Lysophosphatidylserine can be generated from phosphatidylserine. ....	6

### CHAPTER 2: Phosphatidylserine phospholipase A1 enables GPR34-dependent immune cell accumulation in the peritoneal cavity

Figure 2.1. GPR34 KI promotes PC and MemB accumulation in the PerC. ....	17
Figure 2.2. GPR34 KI supports ex vivo lysoPS-mediated chemotaxis, can conditionally promote PerC PC accumulation, and synergizes with BCL2 to enhance PerC MemB abundance. ....	23
Figure 2.3. GPR34 KI promotes MemB proliferation. ....	27
Figure 2.4. GPR34 KI PC and MemB are enriched at the omentum where PLA1A regulates lysoPS abundance. ....	29
Figure 2.5. GPR34 KI PerC PC and MemB maintenance depends on stromal PLA1A... ..	32
Supplementary Figure 2.1. Characterization of GPR34 KI mice. ....	39
Supplementary Figure 2.2. GPR34 deficiency does not result in PC or B cell accumulation defects. ....	41
Supplementary Figure 2.3. GPR34 KI alters gene expression of PerC cells, omental fibroblasts express PLA1A, and GPR34 KI supports PC maintenance in the PerC. ....	42

### CHAPTER 3: Conclusion

Figure 3.1. Model for GPR34 KI PerC PC and MemB accumulation. ....	56
--	----

# **CHAPTER 1**

## **Introduction**

## Peritoneal cavity immunity

The peritoneal cavity (PerC) is a fluid-filled space lined by the peritoneum, a serous membrane that covers the diaphragm, abdominal wall, and abdominal organs (van Baal et al., 2017; Isaza-Restrepo et al., 2018). Among the organs housed by the PerC (**Figure 1.1**), the omentum—a visceral adipose tissue—holds particular importance for immune responses (Liu et al., 2021). In humans, the omentum drapes over the abdominal organs like an apron and has long been noted for its ability to attenuate inflammation and promote the healing of surgical wounds (Meza-Perez and Randall, 2017). Although this adipose tissue is proportionally much smaller in mice, the omenta of both mice and humans contain milky spots, or fat-associated lymphoid clusters (FALCs) (Meza-Perez and Randall, 2017). FALCs are loosely organized collections of B cells, T cells, and myeloid cells that share characteristics of secondary and tertiary lymphoid tissues; they arise as part of normal development at homeostasis, yet they can also be induced in response to the microbiota and inflammatory stimuli (Okabe, 2024). Of various adipose tissues, the omentum has the highest number and density of FALCs (Bénézech et al., 2015), which filter

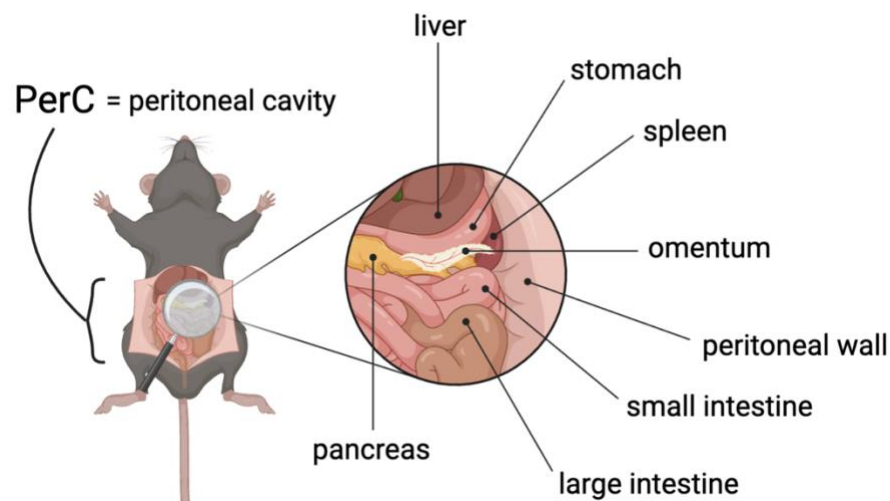


**Figure 1.1. Schematic of the mouse peritoneal cavity.**

Created in BioRender. Adapted from Bella et al., 2021. Select organs in the mouse peritoneal cavity are shown.

the peritoneal fluid and mount local immune responses to encountered antigens and pathogens (Rangel-Moreno et al., 2009; Liu et al., 2021).

PerC immune responses are important during infection and malignancy. Peritonitis, or inflammation of the peritoneum, is an emergent condition often caused by bacterial infection that can lead to life-threatening sepsis with high mortality (Ross et al., 2018; Clements et al., 2021). During peritonitis, there is an increase in the number and size of omental FALCs along with an influx of neutrophils (Cruz-Migoni and Caamaño, 2016; Bénézech et al., 2015). These neutrophils, together with peritoneal macrophages, facilitate pathogen clearance (Jackson-Jones et al., 2020; Leendertse et al., 2009; Vega-Pérez et al., 2021). Strikingly, removal of the omentum leads to worse survival in animal models of peritonitis (Uzunköy et al., 2009; Wang et al., 2019). Even targeted deficiency of innate immunological sensing in stromal cells can increase PerC bacterial spread to the blood and liver (Perez-Shibayama et al., 2018). Beyond bacteria, filarial nematodes, specifically those of the *Mansonella* species, are a prevalent cause of PerC infection in Africa as well as Central and South America (Nanduri and Kazura, 1989; Pietrzak et al., 2024). Although *Mansonella* parasites are thought to have minimal pathogenicity, they evoke a type 2 immune response that may lead to poorer control of tuberculosis and HIV (Ta-Tang et al., 2018; Ritter et al., 2018). Studies of serous cavity filarial infection in mice have revealed that antibody production and myeloid cell recruitment contribute to worm clearance (Rajan et al., 2005; Jackson-Jones et al., 2016; Campbell et al.).

The PerC is also a common site of ovarian and colorectal cancer metastasis associated with poor prognosis (Cortés-Guiral et al., 2021; Coccolini, 2013). In mice, intraperitoneally injected tumor cells localize to omental FALCs (Sorensen et al., 2009; Meza-Perez and Randall, 2017), paralleling patient metastasis patterns (Lengyel et al., 2014). Whereas the omentum has a

critical role in fighting infection, it is generally detrimental for anti-tumor immunity (Liu et al., 2021) due to macrophage subsets that promote tumor survival and proliferation (Rei et al., 2014; Etzerodt et al., 2020). In fact, omentectomy decreases cancer spread in animal models of PerC malignancy (Oosterling et al., 2006; Etzerodt et al., 2020). Nevertheless, there are circumstances under which PerC immune cells enable anti-tumor responses. Stimulated B1 cells produce tumor-specific IgM to trigger complement-mediated tumor killing (Haro et al., 2019). Enrichment of CD103<sup>+</sup> dendritic cells, combined with immune checkpoint blockade, facilitates tumor control (Flies et al., 2016).

In both inflammation and homeostasis, the proper composition, function, and organization of immune cells in omental FALCs depends on a network of fibroblastic stromal cells (Liu et al., 2021; Jackson-Jones and Bénézech, 2020). For example, omental stromal cells generate retinoic acid, which supports the development of large peritoneal macrophages (Okabe and Medzhitov, 2014) and promotes peritoneal B1 cell isotype switching to IgA (Roy et al., 2013). Meanwhile, stroma-derived chemokines mediate immune cell homing to the PerC. CXCL13, produced by omental stromal cells and macrophages, recruits CXCR5<sup>+</sup> B1 cells to body cavities at homeostasis (Ansel et al., 2002). CXCL12 regulation by ALDH1A2<sup>+</sup> fibroblasts is required for the homeostatic maintenance of CXCR4<sup>+</sup> T cells and B2 cells (Yoshihara and Okabe, 2023). After *Salmonella* infection, CCL2, expressed by omental fibroblastic reticular cells, recruits CCR2<sup>+</sup> inflammatory monocytes (Perez-Shibayama et al., 2018). In the context of zymosan-induced peritonitis, CXCL1, produced by mesothelial cells in the omentum, enables the homing of CXCR2<sup>+</sup> neutrophils (Jackson-Jones et al., 2020); CXCL5 may also participate in this process (Song et al., 2013). While a recent study demonstrated that platelet and mast cell derived 5-HIAA influences GPR35<sup>+</sup> neutrophil entry into the inflamed PerC (De Giovanni et al., 2022),

the literature as a whole supports a paradigm where PerC immune cell trafficking primarily depends on chemoattractant ligands generated at least in part by omental stroma.

### **GPR34 is a lysophosphatidylserine receptor**

GPR34 is an X-linked G protein-coupled receptor (GPCR) expressed most abundantly in microglia but also expressed in a variety of other immune cells (Schöneberg et al., 2018). The receptor is  $G_i$ -coupled (Inoue et al., 2019), which canonically supports directed chemotaxis up a ligand gradient (Lu and Cyster, 2019). Indeed, GPR34-transfected cells are pro-migratory towards the GPR34 ligand lysophosphatidylserine (lysoPS) (**Figure 1.2**) (Kitamura et al., 2012). Although there existed conflicting data on whether lysoPS is truly a GPR34 ligand (Schöneberg et al., 2018), three recent cryo-EM studies definitively show the lipid anchored in the ligand-binding pocket of the receptor in complex with the  $G_i$  protein (Xia et al., 2023; Liu et al., 2023; Izume et al., 2024).

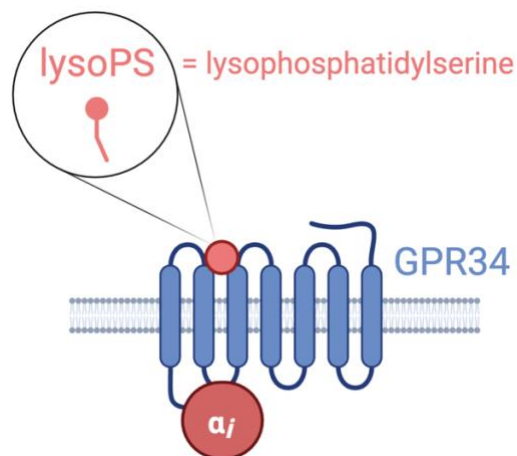


**Figure 1.2 GPR34 is a  $G_i$ -coupled lysophosphatidylserine receptor.**

Created in Biorender. GPR34 is coupled to  $G_i$  and lysophosphatidylserine activates the receptor.

LysoPS can be generated from phosphatidylserine (PS) by PLA1 and PLA2 enzymes that remove one of PS's two fatty acid chains, resulting in the *sn*-2 and *sn*-1 forms of lysoPS, respectively (**Figure 1.3**) (Makide and Aoki, 2013). In vitro, although high concentrations of *sn*-1 lysoPS can activate GPR34, the *sn*-2 form is the more potent ligand, (Kitamura et al., 2012; Uwamizu et al., 2015). Structural docking simulations also suggest that *sn*-2 is likely the physiologically bioactive form (Izume et al., 2024). Of note, in vitro work has shown that *sn*-2 lysoPS is stable only at low pH; at physiological pH, it spontaneously undergoes acyl chain migration to become the *sn*-1 form (Okudaira et al., 2014). Two other X-linked lysoPS receptors, P2RY10 and GPR174, do not share GPR34's *sn*-2 preference, although all three receptors respond most sensitively to lysoPS that contains the 18:1 oleoyl fatty acid side chain (Uwamizu et al., 2015).

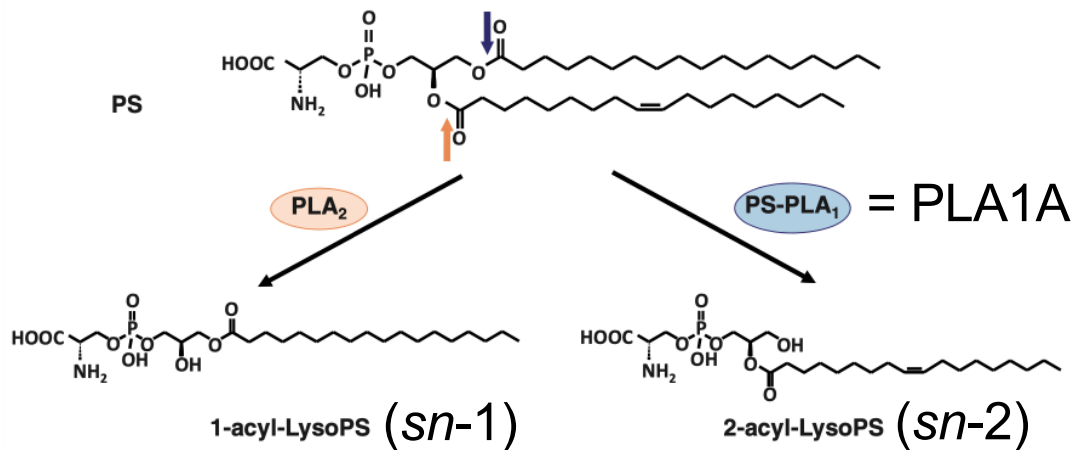


**Figure 1.3. Lysophosphatidylserine can be generated from phosphatidylserine.** Adapted from Makide and Aoki, 2013. PLA2 enzymes generate the *sn*-1 form of lysoPS, whereas PLA1 enzymes generate the *sn*-2 form of lysoPS.

The PS-specific phospholipase A1 (PS-PLA1) enzyme, also known as PLA1A, specifically converts PS into *sn*-2 lysoPS (Zhao et al., 2021). An N-terminal signal sequence

enables secretion of the enzyme into the extracellular space (Aoki et al., 2002) where it acts on PS exposed in the outer leaflet of cell membranes (Makide and Aoki, 2013; Hosono et al., 2001; Izume et al., 2024). PS in healthy cells is normally sequestered on the inner leaflet of the plasma membrane by P4-type ATPases (Leventis and Grinstein, 2010) and is consequently inaccessible to PLA1A (Chakraborty and Kamat, 2024). There are important physiological contexts, however, when PS is flipped to the outer membrane. Perhaps the most well-recognized of these is apoptosis, where cell surface PS exposure triggers engulfment and clearance by phagocytic cells (Leventis and Grinstein, 2010). PS externalization also occurs during platelet activation and hemostasis (Leventis and Grinstein, 2010), on viable cells as part of signal transduction (Segawa et al., 2011; Elliott et al., 2005), and on certain tumor cells (Chang et al., 2020). Inflammatory settings seem to be associated both with increased cell surface PS availability and with elevated levels of PLA1A (Zhao et al., 2021), encouraging the notion that extracellular PLA1A conversion of PS to lysoPS is a physiologically relevant event.

Other than PLA1A, the best defined lysoPS-generating enzyme is ABHD16A, which has PLA2 activity and produces the *sn*-1 form of lysoPS (Chakraborty and Kamat, 2024). Unlike extracellularly secreted PLA1A, ABHD16A is membrane anchored and enriched on the endoplasmic reticulum (ER) (Singh et al., 2020). Its active site faces the cytosol, which facilitates regulation of intracellular lysoPS abundance (Chakraborty and Kamat, 2024). *Abhd16a*<sup>-/-</sup> mice have decreased lysoPS in brain tissue, and enzyme-deficient macrophages show decreased cell-associated and secreted lysoPS in ex vivo culture (Kamat et al., 2015; Singh et al., 2020). Recently, ABHD16B, a distant orthologue of ABHD16A, was described as having PS-specific PLA1 activity based on studies overexpressing human ABHD16B in yeast

(Narayanasamy et al., 2023; Chakraborty and Kamat, 2024). Further investigation is needed to establish the function of ABHD16B in mammalian cells.

Two membrane-anchored serine hydrolases, ABHD12 and ABHD6, have been identified as enzymes that degrade lysoPS in vivo (Chakraborty and Kamat, 2024). ABHD12 is a lysoPS-specific lipase localized at the ER with an active site facing the lumen (Joshi et al., 2018). Mice deficient for ABHD12 have a toxic accumulation of very long chain lysoPS species in the brain that leads to a neurological condition resembling the human disease PHARC (Blankman et al., 2013). Meanwhile, ABHD6 is thought to be a general phospholipase that degrades multiple substrates, only one of which is lysoPS (Thomas et al., 2013). This view was recently challenged by work suggesting that in the liver and kidney, ABHD6 may instead specifically metabolize lysoPS (Chakraborty et al., 2025).

### **Functions of GPR34 in immune cells**

Several in vitro studies with GPR34-transfected cells have shown that lysoPS stimulates various pro-growth signaling pathways (Sugo et al., 2006; Ansell et al., 2012; Korona et al., 2021) in addition to promoting cell migration (Kitamura et al., 2012; Iida et al., 2014). However, prior to the last couple of years, there were relatively few reports of the in vivo function of GPR34 in immune cells. GPR34-deficient mice were first generated over a decade ago and found to have increased delayed type hypersensitivity as well as impaired control of disseminated *Cryptococcus neoformans* infection (Liebscher et al., 2011). Subsequent work suggested that the increased susceptibility of GPR34 knockout mice to brain infection was due to reduced microglial phagocytosis as measured by ex vivo slice cultures (Preissler et al., 2015). A report from a separate group used a nerve injury model to uncover a role for GPR34 in worsening

neuropathic pain, finding correlative evidence that an injury-induced increase of lysoPS activates GPR34 on microglia (Sayo et al., 2019).

An *in vivo*, mechanistic link between lysoPS and GPR34 was missing until several years ago, when Zhou and colleagues found that apoptotic neutrophils release lysoPS at sites of epithelial damage, and that lysoPS signals through GPR34 on type 3 innate lymphoid cells to mediate IL-22-driven tissue repair (Wang et al., 2021). It remained unknown though how apoptotic PS is converted to lysoPS and which of the *sn-1* or *sn-2* isomers activates GPR34 *in vivo*. Since then, Zhou and colleagues have published three additional studies. First, they showed that microglial GPR34 enhances neuroinflammation through AKT and ERK pathways in experimental autoimmune encephalomyelitis and stroke in response to lysoPS in myelin debris (Lin et al., 2024). A related investigation revealed that lysoPS in myelin debris also acts through GPR34 on microglia to promote Alzheimer's disease in a 5xFAD model (Zhou et al., 2025). The third report proposed that type 1 innate lymphoid cells in tumors use GPR34 to inhibit NK tumor-killing activities via lysoPS in the tumor microenvironment (Yan et al., 2024). Surprisingly, the authors implicated PKA and CREB signaling, which are canonically associated with G<sub>s</sub>-coupled rather than G<sub>i</sub>-coupled GPCRs. All three of these studies found that ABHD16A—not PLA1A—is the enzyme responsible for producing lysoPS (Lin et al., 2024; Yan et al., 2024; Zhou et al., 2025). Meanwhile, other groups have investigated PLA1A-deficient mice and suggested that PLA1A-derived lysoPS acts through GPR174—not GPR34 (Zhou et al., 2022; Zhao et al., 2022). Nevertheless, given the compelling evidence that *sn-2* lysoPS is a potent and specific ligand for GPR34 (Kitamura et al., 2012; Uwamizu et al., 2015; Izume et al., 2024), it is worth examining whether PLA1A could be an *in vivo* source of lysoPS that activates GPR34 in other contexts.

In particular, it is speculated that lysoPS generated from PLA1A promotes the progression of human salivary gland (SG) mucosa-associated lymphoid tissue (MALT) lymphomas that harbor recurrent GPR34 mutations (Korona et al., 2021; Moody et al., 2018). These mutations include both translocations—resulting in 10-100-fold elevations in GPR34 transcript—(Baens et al., 2012; Ansell et al., 2012; Akasaka et al., 2017) and putative gain-of-function (GOF) carboxy-terminal (C-terminal) variants (Moody et al., 2018). G<sub>i</sub>-coupled GPCRs are not often thought of as drivers of B cell lymphoma, but there is precedent. Similar C-terminal mutations in CXCR4 and CCR4 are GOF and can lead to malignant transformation in Waldenström macroglobulinemia, a rare lymphoplasmacytic lymphoma, and adult T-cell leukemia/lymphoma, respectively (Martinez-Climent, 2018). Mechanistically, disruption of C-terminal phosphorylation sites causes impaired beta-arrestin recruitment and receptor desensitization, leading to defective termination of pro-growth and cell migration signals (Martinez-Climent, 2018). SG MALT lymphomas are strongly associated with Sjogren’s syndrome, a disease characterized by dry eyes and mouth due to autoimmune destruction of lacrimal and salivary gland tissue (Yang et al., 2025). Sjogren’s patients often have SG lymphoepithelial lesions with B cell infiltration and abundant epithelial cell death (Pringle et al., 2022). PLA1A expressed in these lesions could convert PS from dying cells into lysoPS, creating a ligand-rich environment for GPR34 GOF-harboring B cells to proliferate and transform into lymphoma (Korona et al., 2021). While this hypothesis is logical, it has not been studied in vivo. We thus set out to model GPR34 GOF B cell lymphoma in mice and to explore whether any GPR34 GOF-mediated phenotypes are dependent on *sn-2* lysoPS generated by PLA1A.

## **CHAPTER 2**

# **Phosphatidylserine phospholipase A1 enables GPR34-dependent immune cell accumulation in the peritoneal cavity**

## ABSTRACT

The peritoneal cavity (PerC) is an important site for immune responses to infection and cancer metastasis. Yet few ligand–receptor axes are known to preferentially govern immune cell accumulation in this compartment. GPR34 is a lysophosphatidylserine (lysoPS)-responsive receptor that frequently harbors gain-of-function mutations in mucosa-associated B cell lymphoma. Here, we set out to test the impact of a GPR34 knock-in (KI) allele in the B-lineage. We report that GPR34 KI promotes the PerC accumulation of plasma cells (PC) and memory B cells (MemB). These KI cells migrate robustly to lysoPS *ex vivo*, and the KI allele synergizes with a *Bcl2* transgene to promote MemB but not PC accumulation. Gene expression and labeling studies reveal that GPR34 KI enhances PerC MemB proliferation. Both KI PC and MemB are specifically enriched at the omentum, a visceral adipose tissue containing fibroblasts that express the lysoPS-generating PLA1A enzyme. Adoptive transfer and chimera experiments revealed that KI PC and MemB maintenance in the PerC is dependent on stromal PLA1A. These findings provide *in vivo* evidence that PLA1A produces lysoPS that can regulate GPR34-mediated immune cell accumulation at the omentum.

## INTRODUCTION

The peritoneal cavity (PerC) encloses many abdominal organs, including the omentum, a visceral adipose tissue that contains fat-associated lymphoid clusters (FALCs) (Liu et al., 2021). Also known as milky spots, these unconventional secondary lymphoid tissues are organized by chemokines, filter PerC fluids to collect antigens and cells, and serve as hubs for local immune responses (Ansel et al., 2002; Rangel-Moreno et al., 2009; Bénézech et al., 2015). The proper recruitment, maintenance, and function of PerC immune cells are important in settings of infection (Perez-Shibayama et al., 2018; Christian et al., 2022; Yordanova et al., 2022; Newell et al., 2022) and malignancy (Flies et al., 2016; Haro et al., 2019). Immune cells are generally thought to home to the PerC through the omentum: B1 cells depend on the CXCR5-CXCL13 axis (Ansel et al., 2002), small peritoneal macrophages and inflammatory monocytes use the CCR2-CCL2 axis (Kim et al., 2016; Perez-Shibayama et al., 2018), and neutrophils are recruited by either CXCL5 (Song et al., 2013) or CXCL1 (Jackson-Jones et al., 2020). In each case, the ligand is a protein and is at least in part produced by omental stromal cells. A recent study deviated from this paradigm, showing that GPR35 on neutrophils can influence their recruitment to the inflamed PerC in response to 5-HIAA derived from platelets and mast cells (De Giovanni et al., 2022). Whether additional chemoattractant ligand-receptor pairs direct immune cell trafficking to the PerC is unknown.

GPR34 is an X-linked G protein-coupled receptor (GPCR) that is expressed in various immune cells including both myeloid and lymphoid cells (Schöneberg et al., 2018). Like many chemokine GPCRs that regulate immune cell migration and positioning, GPR34 is G<sub>i</sub>-coupled (Inoue et al., 2019). In vitro work has identified lysophosphatidylserine (lysoPS) as a GPR34 ligand, with the unstable *sn*-2 isomer being more potent than its *sn*-1 counterpart (Kitamura et

al., 2012; Uwamizu et al., 2015). Recent cryo-EM studies have shown lysoPS positioned in the ligand-binding pocket of GPR34 in complex with the G<sub>i</sub> protein (Xia et al., 2023; Liu et al., 2023; Izume et al., 2024), with docking simulations providing structural evidence that *sn*-2 is likely the physiologically bioactive form (Izume et al., 2024). The *sn*-2 isomer of lysoPS can be generated by the secreted phospholipase A1A (PLA1A) enzyme, also known as phosphatidylserine (PS)-PLA1, from PS exposed in the extracellular membrane (Makide and Aoki, 2013; Hosono et al., 2001; Izume et al., 2024). In vitro studies have shown that lysoPS stimulates various pro-growth signaling pathways (Sugo et al., 2006; Ansell et al., 2012; Korona et al., 2021) and induces cell migration (Kitamura et al., 2012) in GPR34-transfected cells.

The in vivo function of GPR34 in immune cells has received only limited study. Reports suggested that GPR34 deficiency compromises host defense against *Cryptococcus neoformans* (Liebscher et al., 2011) and reduces microglial phagocytosis (Preissler et al., 2015). Another showed that, acting in microglia, the receptor worsens neuropathic pain (Sayo et al., 2019). Moreover, it was demonstrated that apoptotic neutrophils at sites of epithelial injury release lysoPS that stimulates GPR34 on type 3 innate lymphoid cells to trigger tissue repair (Wang et al., 2021), although it was unclear how apoptotic PS was converted to lysoPS and whether the *sn*-1 or *sn*-2 isomer was involved. High tissue and serum PLA1A levels have been associated with autoimmune inflammation, cancer, and viral infection (Zhao et al., 2021), but the few studies that show in vivo PLA1A-dependent effects have not implicated GPR34 (Zhou et al., 2022; Zhao et al., 2022).

Perhaps the most prominent GPR34 connection to disease is that GPR34 translocations—associated with 10-100 fold increases in GPR34 transcript abundance—(Baens et al., 2012; Ansell et al., 2012; Akasaka et al., 2017) and putative gain-of-function (GOF) carboxy-terminal

(C-terminal) mutations (Moody et al., 2018) recurrently appear in human salivary gland (SG) mucosa-associated lymphoid tissue (MALT) lymphomas. There is speculation that PLA1A expressed in autoimmune-associated SG lymphoepithelial lesions may generate lysoPS that contributes to the outgrowth of GPR34 GOF-harboring tumor cells (Korona et al., 2021). SG MALT lymphomas are neoplasms of marginal zone B cells (MZB) (Troppan et al., 2015), which are B lymphocytes named for their localization along the border of the red and the white pulp of the spleen but also found in non-lymphoid target tissues in autoimmune disease (Palm and Kleinau, 2021). Although MZB are distinct from classical memory B cells (MemB), MZB have memory properties in that they can also rapidly activate and differentiate into antibody-secreting plasma cells (PC) upon antigen encounter (Cerutti et al., 2013). While GPR34 translocations and GOF mutations are enriched in SG cases (Moody et al., 2018), GPR34 expression is generally increased in MALT, MZB, and lymphoplasmacytic lymphomas (Ansell et al., 2012), suggesting a broader pathological relevance of the receptor.

In an effort to model human lymphoma, we generated B cell-specific GPR34 GOF knock-in (KI) mice. Our analyses of these mice revealed an unexpected accumulation of PC and MemB in the PerC. We report that ex vivo PerC KI cells strongly migrate to lysoPS and that GPR34 KI augments PerC MemB proliferation. PLA1A was found to produce *sn-2* lysoPS at the omentum, where KI PC and MemB are enriched. We show that stromal-derived enzyme is required for the GPR34-dependent maintenance of KI cells in the PerC.

## RESULTS AND DISCUSSION

### Generation of GPR34 GOF KI mice

Truncations are common among the C-terminal GPR34 mutations in SG MALT lymphoma (Moody et al., 2018). Of note, similar mutations in other GPCRs, in particular CXCR4 and CCR4, are GOF and can lead to malignant transformation (Martinez-Climent, 2018). To test the functional effect of GPR34 truncations, we retrovirally transduced either mouse R337X or wild-type (WT) GPR34 into the WEHI-231 mouse B lymphoma cell line. In accord with a report using transfected epithelial cells (Kitamura et al., 2012), overexpression of WT GPR34 enabled concentration-dependent transwell migration of WEHI-231 cells to lysoPS (**Supplementary Figure 2.1 A**). Meanwhile, R337X exhibited GOF behavior with a larger and more sensitive response (**Supplementary Figure 2.1 A**) in line with the enhanced signaling and growth properties of a different C-terminal truncation (Korona et al., 2021). Attempts to study both the WT and GOF versions of the receptor in vivo through retroviral overexpression bone marrow (BM) chimeras were limited by plasmid toxicity effects that made the GPR34 construct unstable and prone to mutation during growth in bacteria (unpublished data). As an alternative approach, we generated mice harboring a conditional GPR34 GOF KI allele with a GFP reporter (**Figure 2.1 A**). For this model, we chose mouse Q340X, which is homologous to human Q347X, the most frequent GPR34 mutation found in SG MALT lymphoma (Moody et al., 2018). In *Cd21<sup>Cre</sup>R26<sup>LSL-Gpr34Q340X-IRES-GFP</sup>*—henceforth “KI”—mice, reporter expression in the hematopoietic compartment was restricted to B-lineage cells (**Supplementary Figure 2.1 B**). Consistent with previous studies of *Cd21<sup>Cre</sup>*-mediated recombination efficiency (Kraus et al., 2004), the KI allele was expressed in ~80% of splenic follicular B cells (FoB) (**Supplementary Figure 2.1 C**).

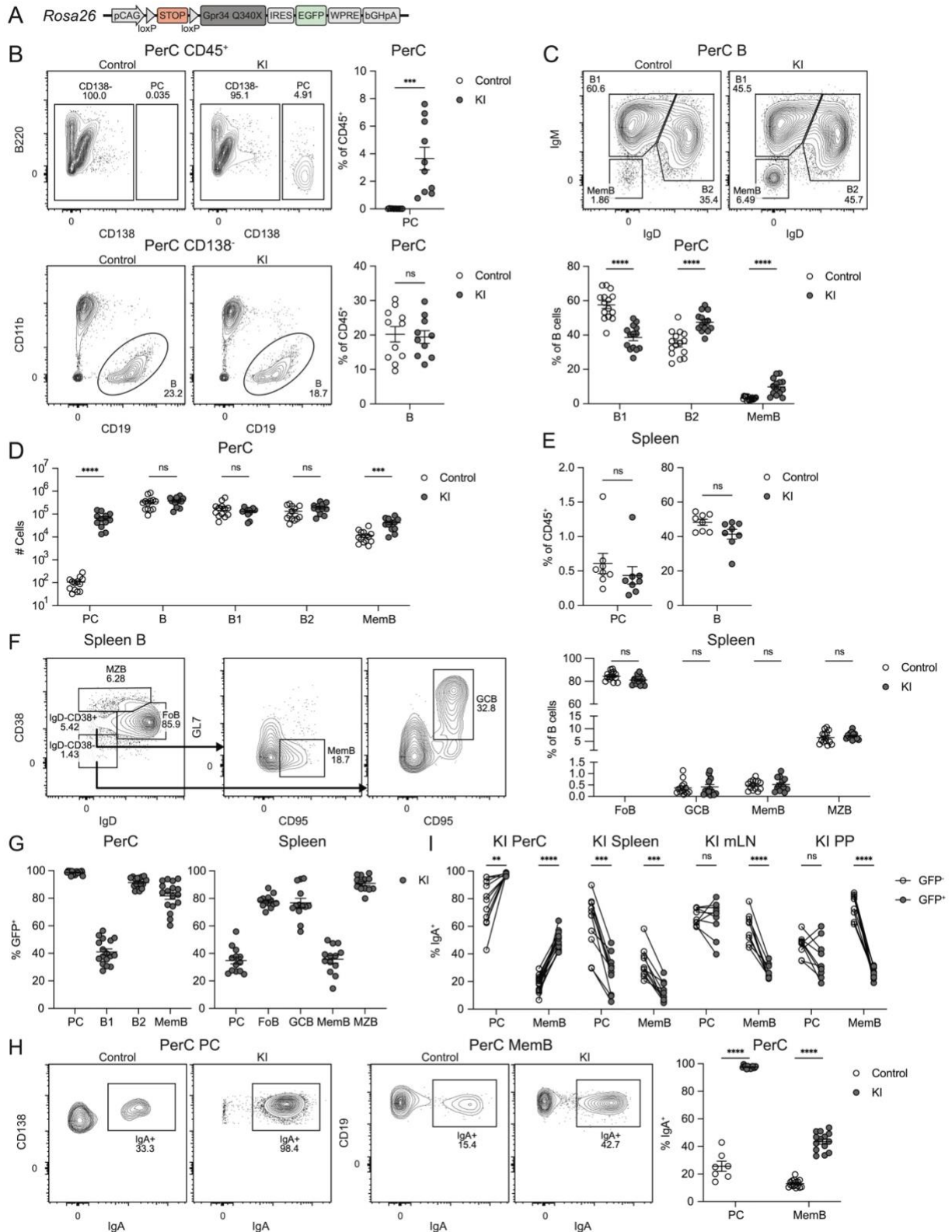


**Figure 2.1. GPR34 KI promotes PC and MemB accumulation in the PerC.**  
**(A)** Diagram of the GPR34 GOF conditional KI allele situated at the *Rosa26* locus. **(B-I)**  
 (Figure caption continued on the next page.)

(Figure caption continued from the previous page.)

Immune cells from control and KI (*Cd21<sup>Cre</sup>R26<sup>LSL-Gpr34Q340X-IRES-GFP</sup>*) mice were analyzed by flow cytometry. **(B)** Left top: Representative flow cytometry plots of PerC CD45<sup>+</sup> cells gated for PC (CD138<sup>+</sup>) and annotated with PC frequency. Left bottom: Representative flow cytometry plots of PerC CD45<sup>+</sup>CD138<sup>-</sup> cells gated for B cells (CD19<sup>+</sup>) and annotated with B cell frequency. Right: Percentages of PerC PC and B cells amongst CD45<sup>+</sup> cells (control, *n* = 11; KI, *n* = 10). **(C)** Top: Representative flow cytometry plots of PerC B cells gated for B1 (IgD<sup>-</sup>IgM<sup>+</sup>), B2 (IgD<sup>+</sup>IgM<sup>+</sup>), and MemB (IgD<sup>-</sup>IgM<sup>-</sup>) and annotated with subset frequencies. Bottom: Percentages of PerC B1, B2, and MemB amongst B cells (control, *n* = 15; KI, *n* = 14). **(D)** Cell numbers of the indicated populations in the PerC (control, *n* = 13; KI, *n* = 12). **(E)** Frequencies of the indicated populations in the spleen (control, *n* = 8; KI, *n* = 8). **(F)** Left: Representative flow cytometry plots showing the gating scheme for spleen FoB (IgD<sup>+</sup>CD38<sup>+</sup>), GCB (IgD<sup>-</sup>CD38<sup>-</sup>GL7<sup>+</sup>CD95<sup>+</sup>), MemB (IgD<sup>-</sup>CD38<sup>+</sup>GL7<sup>-</sup>CD95<sup>+</sup>), and MZB (IgD<sup>int</sup>CD38<sup>hi</sup>). Right: Percentages of FoB, GCB, MemB, and MZB amongst spleen B cells (control, *n* = 14; KI, *n* = 14). **(G)** Frequencies of GFP<sup>+</sup> cells within the indicated populations in the PerC and spleen (PerC, *n* = 17; spleen, *n* = 13). **(H)** Left: Representative flow cytometry plots of PerC PC and MemB gated for IgA<sup>+</sup> cells and annotated with IgA<sup>+</sup> frequency. Right: Percentages of IgA<sup>+</sup> cells within the indicated populations in the PerC (control PC, *n* = 7; control MemB, *n* = 15; KI, *n* = 14). **(I)** Frequencies of IgA<sup>+</sup> cells within the GFP<sup>-</sup> and GFP<sup>+</sup> subsets of the indicated populations in KI mice (PerC PC, *n* = 11; PerC MemB, *n* = 15; spleen, *n* = 10; mLN, *n* = 9; PP, *n* = 9). In B-H, each data point represents an individual mouse, lines indicate means, and error bars represent SEM. In I, each pair of connected points represents data from one mouse. Data were pooled from three or more independent experiments. Statistical significance was determined by unpaired *t* test (B-F and H) or paired *t* test (I) corrected for multiple comparisons (Holm-Šídák). ns, not significant; \*\**P* < 0.01; \*\*\**P* < 0.001; \*\*\*\**P* < 0.0001.

## GPR34 KI promotes the PerC accumulation of PC and MemB

Flow cytometric profiling of KI mice at homeostasis revealed normal numbers of B cells in the spleen and inguinal lymph nodes (iLN) (**Supplementary Figure 2.1 D**). Analysis of the SG identified very few B cells in control mice and no accumulation in the GPR34 GOF setting (**Supplementary Figure 2.1 D**). Profiling of B-lineage cells in additional tissues revealed a marked accumulation of KI PC in the PerC. While CD138<sup>+</sup> PC were virtually absent from the PerC of controls, they constituted ~3% of PerC immune cells in KI mice (**Figure 2.1 B**). Within B cells, we observed a relative decrease in B1 (IgD<sup>-</sup>IgM<sup>+</sup>) and a relative increase in B2 (IgD<sup>+</sup>IgM<sup>+</sup>) and class-switched MemB (IgD<sup>-</sup>IgM<sup>-</sup>), but the overall B cell frequency was unaffected (**Figure 2.1, B and C**). Numerically, there was a ~500-fold increase in PC and an approximately threefold increase in MemB (**Figure 2.1 D**). Outside of the B-lineage, *Cd21<sup>Cre</sup>* is active in stromal follicular dendritic cells. We reconstituted WT mice with BM from KI donors and found similar PerC accumulation of PC and MemB (**Supplementary Figure 2.1 E**), indicating that the observed phenotypes are B cell intrinsic.

In contrast to the PerC, PC and MemB were not expanded in the spleen (**Figure 2.1, E and F**). Splenic FoB, germinal center B cells (GCB), and MZB were also unaffected (**Figure 2.1 F**). We observed lower KI GFP reporter positivity for splenic PC and MemB relative to their counterparts in the PerC (**Figure 2.1 G**). To a lesser extent, there was also lower KI GFP<sup>+</sup> frequency amongst splenic FoB compared to PerC B2 (**Figure 2.1 G**). The high GFP reporter positivity in splenic MZB (**Figure 2.1 G**) is in accord with high *Cd21<sup>Cre</sup>* activity in these CD21<sup>hi</sup> cells. The enrichment of GFP<sup>+</sup> PC, MemB, and B2 in the PerC compared to spleen is consistent with the GPR34 GOF allele promoting accumulation of these cell types in the PerC.

We found that PerC KI PC were nearly 100% IgA<sup>+</sup> (**Figure 2.1 H**) and expressed CCR9 (**Supplementary Figure 2.1 F**), which are properties of gut-associated PC (Pabst et al., 2004). PerC KI MemB also had increased IgA positivity (**Figure 2.1 H**), and within KI mice, GFP<sup>+</sup> PerC PC and MemB had higher IgA<sup>+</sup> percentages than their GFP<sup>-</sup> counterparts (**Figure 2.1 I**). With one exception, no significant IgA<sup>+</sup> frequency differences were identified in other surveyed organs at the gross population level (**Supplementary Figure 2.1 G**). These data make it unlikely that the GPR34 GOF allele is directly promoting IgA class switching. Subsetting by GFP positivity revealed lower IgA<sup>+</sup> proportions within reporter-positive spleen PC and MemB as well as MemB in the mesenteric LN (mLN) and the Peyer's patches (PP) (**Figure 2.1 I**). Additionally, we observed lower frequencies and low GFP<sup>+</sup> percentages of KI PC and MemB in the PP (**Supplementary Figure 2.1, H-J**).

While control IgA<sup>+</sup> PC home via the circulation preferentially to the small intestine (SI) lamina propria (LP) (Isho et al., 2021), their KI counterparts may instead be diverted to the PerC. This aligns with the observation that only ~5% of KI SI LP PC were GFP<sup>+</sup> compared to ~30% in the PP (**Supplementary Figure 2.1 J**), revealing a strong bias against KI PC accumulation in the gut LP. SI LP PC abundance did not significantly differ between KI and control (**Supplementary Figure 2.1 H**), indicating that reporter negative IgA<sup>+</sup> PC fill the niche. Comparison across organs highlights the PerC as the site with the largest PC and MemB frequency differences (**Supplementary Figure 2.1, H and I**) and the strongest enrichment for KI reporter expression (**Supplementary Figure 2.1 J**), consistent with the PerC being a destination of IgA<sup>+</sup> KI PC and MemB. The pleural cavity (PleuralC) shares certain immunological properties with the PerC (Ansel et al., 2002) and we observed that KI PC but not MemB had increased frequency,

increased IgA positivity, and high GFP reporter positivity at this site (**Supplementary Figure 2.1, G-J**).

Although the mLN showed a reduction in the IgA<sup>+</sup> MemB amongst the GFP<sup>+</sup> KI population (**Figure 2.1 I**), there was an increased frequency and high GFP positivity of KI PC in this tissue (**Supplementary Figure 2.1, H and J**). High GFP positivity was also observed amongst PCs and MemB in the cervical LN (cLN) (**Supplementary Figure 2.1 J**). These data suggest there may be additional effects of the KI allele beyond those on IgA<sup>+</sup> cells that influence cell migration or persistence in lymphoid tissues.

### **PC and B cell abundance are unaltered in GPR34-deficient mice**

Given the phenotypes observed with GPR34 GOF overexpression, we wondered if GPR34 deficiency would result in defects in PC or MemB populations. Surface staining for GPR34 using a polyclonal antibody demonstrated that WT PerC MemB expressed a low level of the receptor (**Supplementary Figure 2.2 A**), consistent with transcriptional data for MemB in the spleen (Bhattacharya et al., 2007; Duan et al., 2021). GPR34 protein was not detected on WT B1, B2, or PC (**Supplementary Figure 2.2 A**). As expected, cells from KI mice exhibited strong GPR34 protein expression (**Supplementary Figure 2.2 A**). At homeostasis, there was no reduction of PerC PC and MemB frequencies in GPR34-deficient mice (**Supplementary Figure 2.2 B**). Intraperitoneal (IP) immunization with nitrophenyl haptenated keyhole limpet hemocyanin (NP-KLH) in alum adjuvant induced an overall increase in PerC PC at 2 wk but did not reveal any GPR34-dependent changes in PC or B cell frequency (**Supplementary Figure 2.2 C**). PC and B cell abundance also did not differ in the spleen, mLN, and PP at homeostasis

(**Supplementary Figure 2.2, D and E**). These results indicate that endogenous levels of GPR34 on MemB are insufficient to alter B cell population frequencies in the contexts we studied.

### **GPR34 KI cells migrate to lysoPS ex vivo**

To investigate whether chemotaxis may contribute to the accumulation of KI cells in the PerC, we first evaluated their transwell migration to various chemoattractants. Both control and KI B2 and MemB responded to CXCL13, but only the KI populations migrated to lysoPS (**Figure 2.2 A**). KI PC also showed migration towards the CCR9 ligand CCL25 (**Figure 2.2 A**), agreeing with CCR9 expression levels (**Supplementary Figure 2.1 F**). We next tested whether intravenously (IV) transferred KI cells could home to the PerC (**Figure 2.2 B**). Regardless of their genotype or anatomical origin, at three days after IV transfer, donor B cells, PC, and MemB were less recovered from the PerC than from the spleen; in particular, donor KI PC were not detected in the PerC of recipients, and donor KI MemB showed no homing advantage over their control counterparts (**Figure 2.2 C**). Our inability to observe KI PC trafficking from the blood into the PerC may be explained by limited donor cell numbers and altered properties of ex vivo-manipulated cells. Inefficient entry into the PerC in short term homing assays (**Figure 2.2, B and C**) might be counteracted in KI mice by a continuous flux of KI cells through the circulation. It is also possible that KI PC and MemB arrive in the PerC via a non-hematogenous route or that they develop locally in the PerC.

### **Conditional activation of GPR34 KI is sufficient for PerC PC accumulation**

Both PC and MemB are prominently affected in the *Cd21<sup>Cre</sup>* model, which promotes expression of the GOF receptor at the mature B cell stage. To assess the effect of expressing

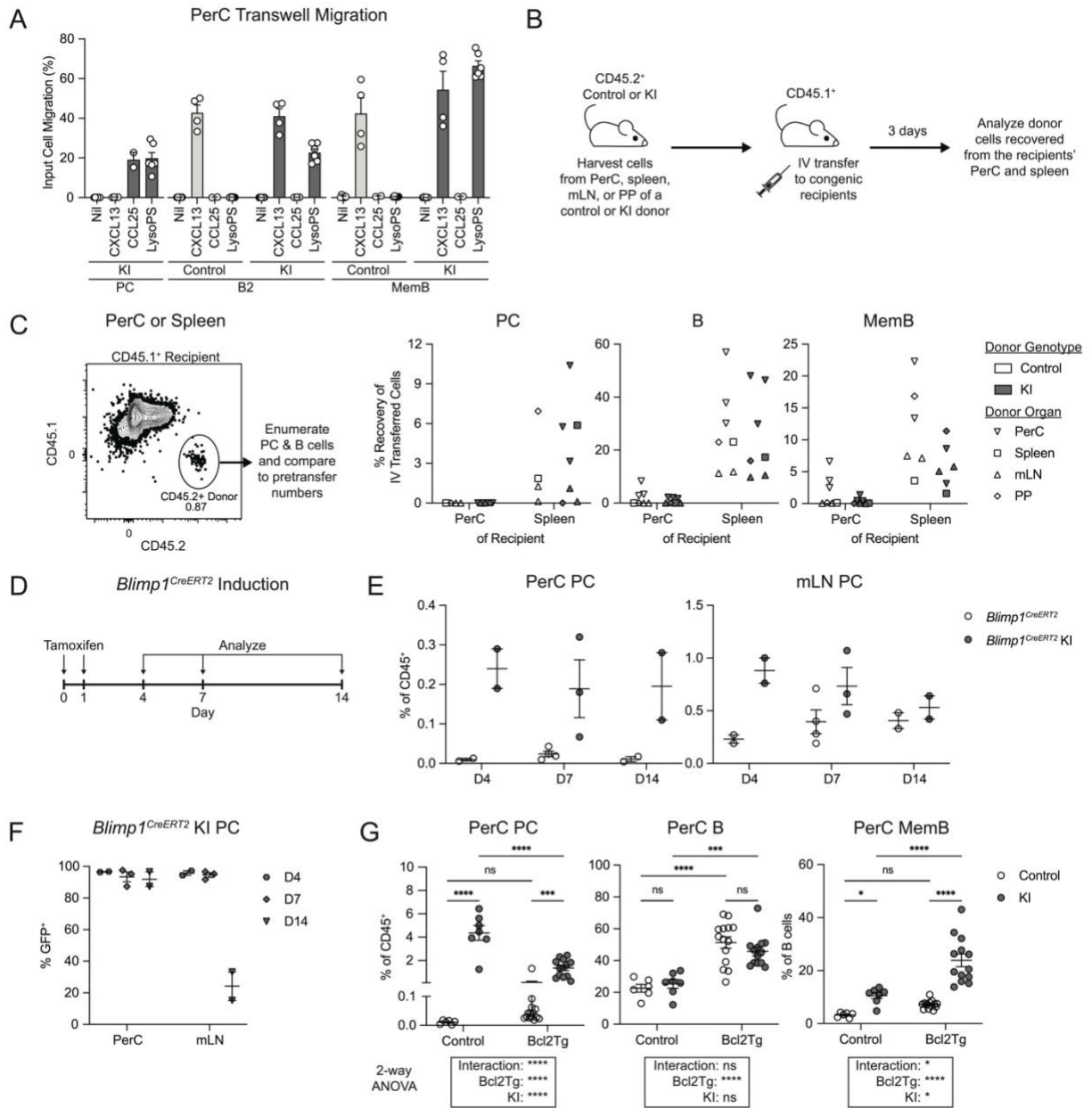


**Figure 2.2. GPR34 KI supports ex vivo lysoPS-mediated chemotaxis, can conditionally promote PerC PC accumulation, and synergizes with BCL2 to enhance PerC MemB abundance.**

(A) PerC cells were harvested from control and KI (*Cd21*<sup>Cre</sup>*R26*<sup>LSL-Gpr34Q340X-IRES-GFP) mice and assayed for transwell migration to 1  $\mu$ g/ml CXCL13, 5  $\mu$ g/ml CCL25, or 5  $\mu$ M lysoPS 18:1. Bar graph shows the frequency of PC (CD138<sup>+</sup>), B2 (IgD<sup>+</sup>IgM<sup>+</sup>), and MemB (IgD<sup>-</sup>IgM<sup>-</sup>) migration relative to input (nil, *n* = 6; CXCL13, *n* = 4; CCL25, *n* = 2; LysoPS, *n* = 6). (B-G) Immune cells were analyzed by flow cytometry. (B and C) PerC, spleen, mLN, and PP cells were harvested from control and KI mice, followed by adoptive transfer IV into congenic recipients. 3 days later, recipients' PerC and spleen were analyzed for donor cells. (B) Schematic of IV adoptive transfer experiment. (C) Left: Representative flow cytometry plot identifying CD45.2<sup>+</sup> congenic donor (Figure caption continued on the next page.)</sup>

(Figure caption continued from the previous page.)

cells in samples harvested from CD45.1<sup>+</sup> recipients. Right: Plots show the percent of pretransfer donor cells recovered from the recipients' PerC and spleen. PerC donor MemB were gated as IgD<sup>-</sup>IgM<sup>-</sup> and donor MemB from other organs were gated as IgD<sup>-</sup>CD38<sup>+</sup> (control,  $n = 6-7$ ; KI,  $n = 6-7$ ; donor control PerC PC abundance was insufficient for quantification of their recovery from recipients). **(D-F)** *Blimp1*<sup>CreERT2</sup> and *Blimp1*<sup>CreERT2</sup> KI (*Blimp1*<sup>CreERT2</sup>*R26*<sup>LSL-GPR34Q340X-IRES-GFP</sup>) BM chimeric mice received tamoxifen via oral gavage on days 0 and 1 and were analyzed on days 4, 7, or 14 (D4,  $n = 2$ ; D7,  $n = 3-4$ ; D14,  $n = 2$ ). **(D)** Timeline of tamoxifen induction and analysis. **(E)** Frequency of PerC and mLN PC at the indicated timepoints. **(F)** Frequency of GFP<sup>+</sup> cells within PerC and mLN PC at the indicated timepoints. **(G)** Frequency of the indicated PerC populations in control and KI mice with or without the *Eμ-Bcl2* transgene (control,  $n = 6$ ; KI,  $n = 7$ ; Bcl2Tg,  $n = 14$ ; Bcl2Tg KI,  $n = 13$ ). Each data point represents an individual transwell (A) or mouse (C and E-G), lines indicate means, and error bars represent SEM. Data were pooled from three independent experiments, except in E and F, which were pooled from two experiments. Statistical significance (G) was determined by two-way ANOVA, followed by multiple comparisons using Fisher's LSD test. ns, not significant; \*P < 0.05; \*\*\*P < 0.001; \*\*\*\*P < 0.0001.

GPR34 KI specifically at the PC stage, we bred the KI allele with *Blimp1<sup>CreERT2</sup>* mice that also have a tdTomato reporter at the *Blimp1* locus (Robinson et al., 2023). 8 wk after reconstitution, *Blimp1<sup>CreERT2</sup>R26<sup>LSL-GPR34Q340X-IRES-GFP</sup>* BM chimeric mice—“Blimp1Cre KI”—received tamoxifen via oral gavage on days 0 and 1, followed by analysis at various timepoints (**Figure 2.2 D**). By day 4, Blimp1Cre KI PC were strongly accumulated in the PerC, though at a frequency ~10-fold lower than in the *Cd21<sup>Cre</sup>* model; this level persisted at least through day 14 (**Figure 2.2 E**). An increase in mLN PC was also present at day 4 but subsequently waned (**Figure 2.2 E**). These data correlated with the maintenance of high Blimp1Cre KI PC GFP reporter positivity in the PerC even after it dropped in the mLN pursuant to tamoxifen clearance (**Figure 2.2 F**). Thus, GPR34 KI can conditionally promote PerC PC accumulation when turned on at the PC stage, and KI PC selectively persist in the PerC after seeding.

### **KI PerC MemB accumulation is enhanced by Bcl2 overexpression**

To explore the interaction of cell survival signals with the maintenance of PerC PC and MemB, we used *Eμ-bcl2* mice (Strasser et al., 1991), in which anti-apoptotic Bcl2 protein is expressed in the B-lineage, leading to overall expansion of B cells, including the splenic PC and MemB compartments (Smith et al., 1994, 2000). In the PerC, there were trends for increases in both PC and MemB in Bcl2 transgenic compared to control mice (**Figure 2.2 G**). On a GPR34 KI background, addition of the Bcl2 transgene decreased PC frequency but increased MemB abundance, with a significant interaction between the genotypes indicating a greater than additive effect (**Figure 2.2 G**). These data reveal that in the context of PerC MemB accumulation, GPR34 KI provides signals that are non-redundant with Bcl2. Furthermore, there exists at least one condition in which KI PC and MemB can be regulated in opposing directions.

### **GPR34 KI enhances MemB proliferation**

Given previous reports of GPR34's pro-growth properties in vitro (Ansell et al., 2012; Jin et al., 2015), we wondered if PerC KI cells have increased cell proliferation. PerC B2 and MemB were sorted from control and KI mice for bulk RNA sequencing (RNAseq). Principal component analysis (PCA) revealed prominent transcriptional differences between B2 and MemB along PC1; control and KI B2 were relatively similar, while PC2 captured differences between control and KI MemB (**Figure 2.3 A**). Consistently, there were a much greater number of differentially expressed genes (DEGs) when comparing KI versus control MemB than when comparing KI versus control B2 (**Supplementary Figure 2.3, A and B**). Gene Ontology (GO) analysis of genes upregulated in KI MemB revealed enrichment for terms associated with "cell division" (**Figure 2.3 B**). Accordingly, many cell cycle related transcripts, including *Cdc45*, *Cdk1*, *Cdkn1a*, and *Mki67* were upregulated (**Figure 2.3 C**). Intracellular staining confirmed an elevated frequency of Ki67<sup>+</sup> MemB in KI compared with control (**Figure 2.3 D**). KI PC, B1, and B2 did not exhibit this increase, although PC Ki67 levels were generally high (**Figure 2.3 D**). As an orthogonal measurement of cell proliferation, we administered a single IP pulse of 5-ethynyl-2'-deoxyuridine (EdU) 90 minutes before analysis. KI MemB incorporated more EdU than their control counterparts, with the PC, B1, and B2 populations largely unaffected (**Figure 2.3 E**).

### **The omentum is enriched for KI PC and MemB**

We next asked whether KI PerC cells were equivalently distributed across the surfaces of PerC organs. Rinsing off surface-associated cells from various tissues revealed a striking enrichment of KI PC and MemB at the omentum (**Figure 2.4 A**). The omentum is a hub for local PerC immunity (Rangel-Moreno et al., 2009; Perez-Shibayama et al., 2018), and previous studies

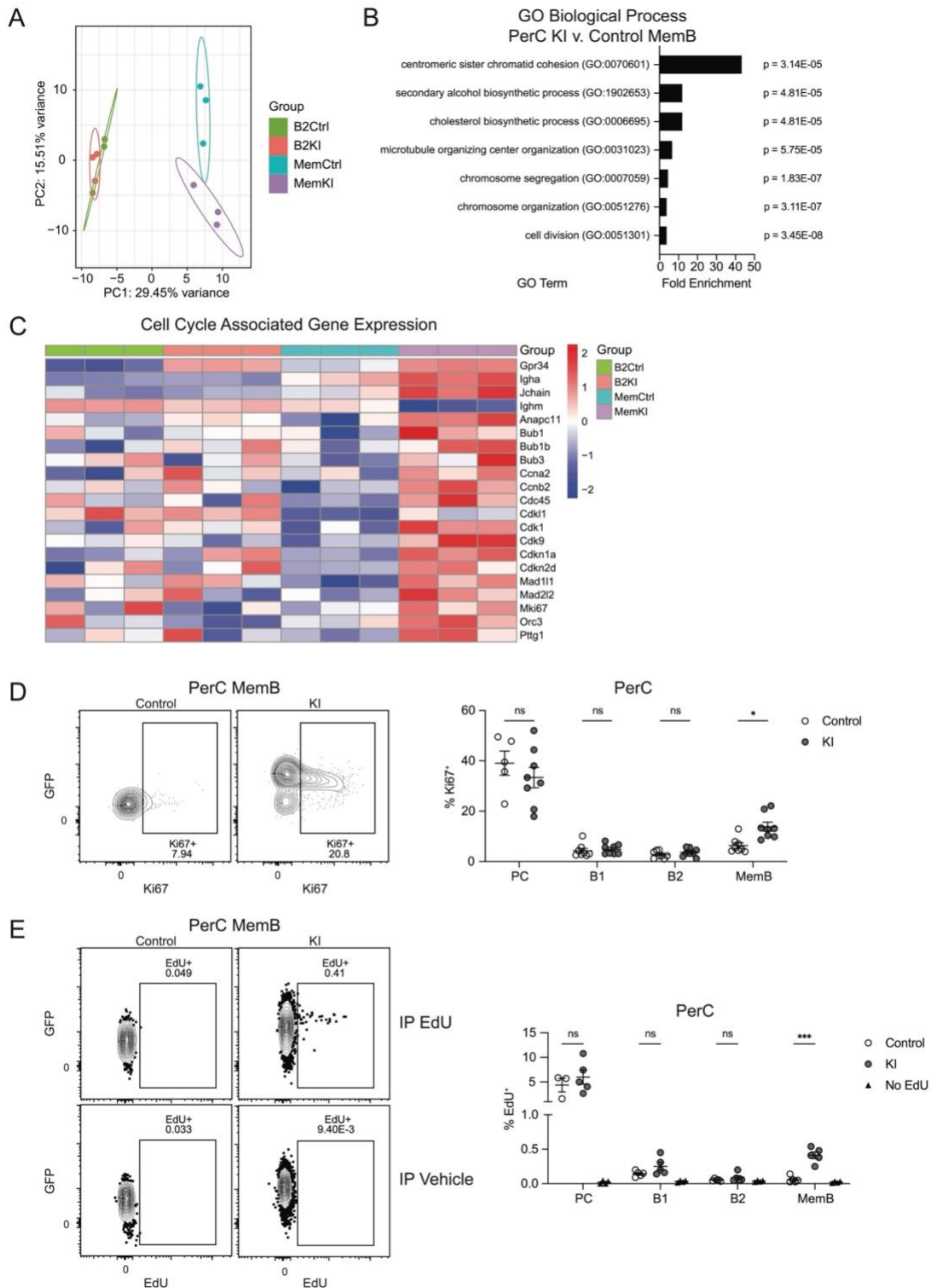


**Figure 2.3. GPR34 KI promotes MemB proliferation.**

(A-C) B2 (IgD<sup>+</sup>IgM<sup>+</sup>) and MemB (IgD<sup>-</sup>IgM<sup>-</sup>) cells were sorted from the PerC from control and KI (*Cd21<sup>Cre</sup>R26<sup>LSL-Gpr34Q340X-IRES-GFP</sup>*) mice for bulk RNAseq (control B2,  $n = 3$ ; control MemB,  $n = 3$ ; KI B2,  $n = 3$ ; KI MemB,  $n = 3$ ). (A) PCA plot of sequencing samples. (B) GO analysis of (Figure caption continued on the next page.)

(Figure caption continued from the previous page.)

top upregulated DEGs comparing KI MemB to control MemB. Bar graph shows the seven GO terms with the highest fold enrichment along with each term's P value. **(C)** Heatmap comparing normalized expression of *Gpr34*, *Igha*, *Jchain*, *Ighm*, and selected cell cycle-associated genes across the indicated populations. **(D and E)** Immune cells from control and KI mice were analyzed by flow cytometry. **(D)** Left: Representative flow cytometry plots of PerC MemB gated for Ki67<sup>+</sup> cells and annotated with Ki67<sup>+</sup> frequency. Right: Percentages of Ki67<sup>+</sup> cells within PerC PC (CD138<sup>+</sup>), B1 (IgD<sup>+</sup>IgM<sup>+</sup>), B2, and MemB (control PC, *n* = 5; other control, *n* = 8; KI, *n* = 8). **(E)** Left: Representative flow cytometry plots of PerC MemB gated for EdU<sup>+</sup> cells and annotated with EdU<sup>+</sup> frequency. Right: Percentages of EdU incorporation in the indicated PerC populations 90 minutes after IP injection of EdU or vehicle (control PC, *n* = 3; other control, *n* = 5; KI, *n* = 5; no EdU, *n* = 4). Each data point represents an individual mouse (D and E), lines indicate means, and error bars represent SEM. Data were pooled from three (D) or two (E) independent experiments. Statistical significance (D and E) was determined by unpaired *t* test corrected for multiple comparisons (Holm-Šidák). ns, not significant; \**P* < 0.05; \*\*\**P* < 0.001.

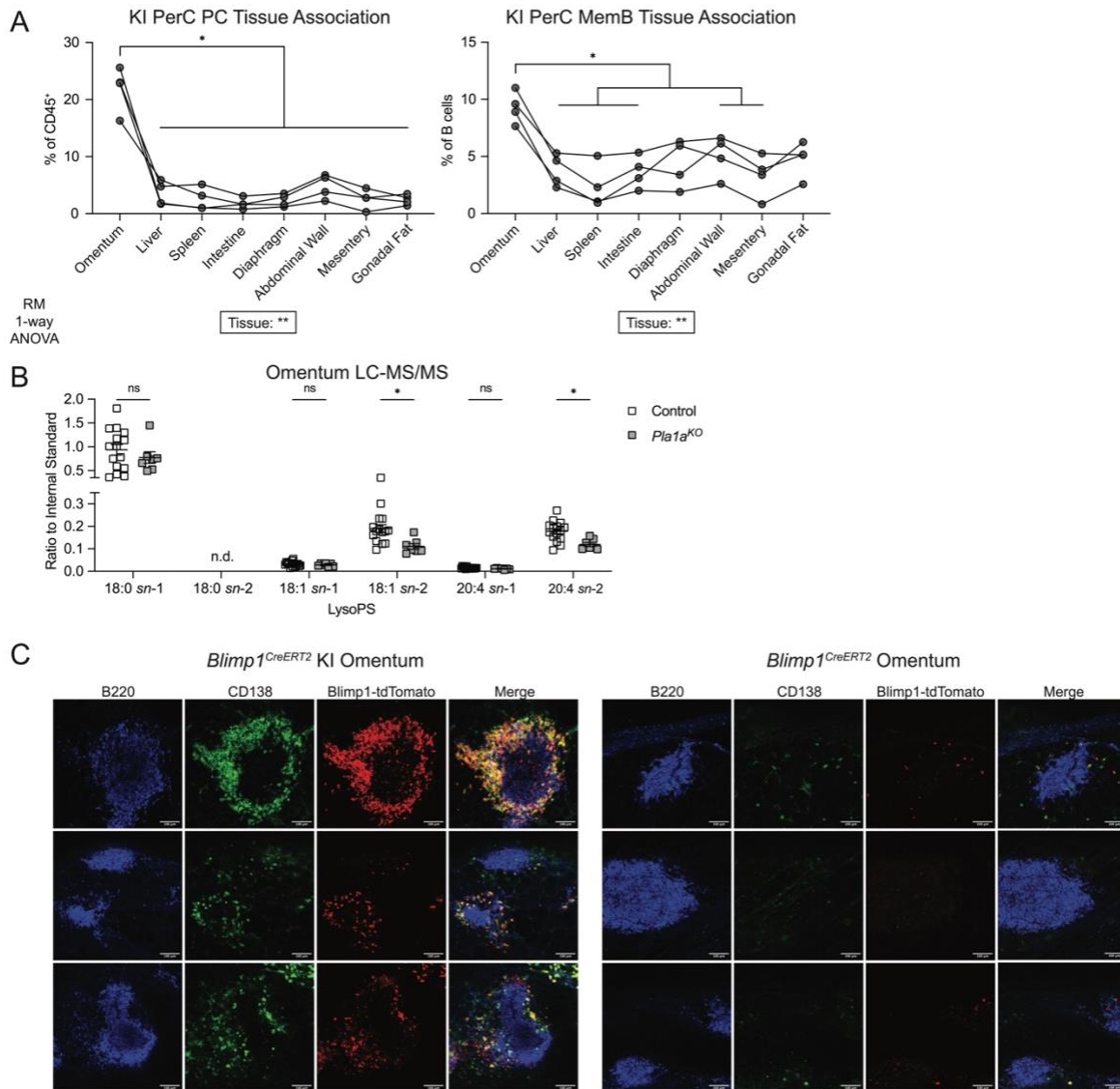


**Figure 2.4. GPR34 KI PC and MemB are enriched at the omentum where PLA1A regulates lysoPS abundance.**

(A) PerC organs from KI (*Cd21*<sup>Cre</sup>*R26*<sup>LSL-Gpr34Q340X-IRES-GFP</sup>) mice or KI BM chimeric mice were harvested and rinsed in MACS buffer to dissociate cells physically associated with the visceral peritoneal surface of each tissue. Plots show frequencies of PC (CD138<sup>+</sup>) and MemB (IgD<sup>+</sup>IgM<sup>-</sup>) in these tissue rinses analyzed by flow cytometry. Each set of connected points represents data from one mouse ( $n = 4$ ). Data are pooled from two independent experiments. Statistical significance was determined by repeated measures one-way ANOVA with the Geisser-Greenhouse correction, followed by paired  $t$  test of each tissue to the omentum corrected for multiple comparisons (Holm-Šidák). (B) LC-MS/MS quantification of the indicated *sn-1* and *sn-2* lysoPS species in the homogenized omentum of control (*Pla1a*<sup>WT</sup> or <sup>Het</sup>) and *Pla1a*<sup>KO</sup> mice (control,  $n = 15$ ; *Pla1a*<sup>KO</sup>,  $n = 7$ ). Data were normalized to an internal standard. Each data point represents an individual mouse, lines indicate means, and error bars represent SEM. Data are pooled from two independent experiments. Statistical significance was determined by unpaired  $t$  (Figure caption continued on the next page.)

(Figure caption continued from the previous page.)

test corrected for multiple comparisons (Holm-Šídák). (C) Representative immunofluorescence images of omenta from *Blimp1*<sup>CreERT2</sup> KI (*Blimp1*<sup>CreERT2</sup>*R26*<sup>LSL-GPR34Q340X-IRES-GFP</sup>) ( $n = 3$ ) and *Blimp1*<sup>CreERT2</sup> control mice ( $n = 2$ ) 4 days after tamoxifen treatment. PC are CD138<sup>+</sup>*Blimp1*-tdTomato<sup>+</sup>. Images are focused on individual FALCs, and three examples from each strain are shown. Images were pooled from three independent experiments. Scale bar 100  $\mu$ m. n.d., not detected; ns, not significant; \* $P < 0.05$ .

have shown that omental stroma express chemokines to recruit immune cells (Ansel et al., 2002; Jackson-Jones et al., 2020). While the rinsing data do not demonstrate that the KI cells entered the PerC through the omentum, they are consistent with this possibility. To explore whether the GPR34 ligand lysoPS is likely to be produced at the omentum, we reanalyzed a published single-cell RNAseq (scRNAseq) dataset of omental stromal cells (Jackson-Jones et al., 2020) and found that transcripts of the lysoPS-generating enzyme PLA1A were well-expressed in the *Ccl11<sup>+</sup>Pdgfra<sup>+</sup>* fibroblast subset (**Supplementary Figure 2.3 C**). On the whole-tissue level, *Plala* transcripts were significantly more abundant in the omentum than in the SG and spleen (**Supplementary Figure 2.3 D**). Liquid chromatography-tandem mass spectrometry (LC-MS/MS) quantification of lysoPS revealed that omentum tissue from *Plala<sup>KO</sup>* mice contained a lower abundance of *sn-2* 18:1 and 20:4 while the *sn-1* forms were unchanged (**Figure 2.4 B**). The remaining *sn-2* lysoPS detected in PLA1A-deficient mice may be an artifact of sample preparation or may truly reflect in vivo levels, although it is unclear if there exist additional *sn-2* lysoPS-generating enzymes (Omi et al., 2021). In our efforts to reliably identify KI PC on the omentum by immunofluorescence whole-mount microscopy, we were greatly aided by the Blimp1-tdTomato reporter. In Blimp1Cre KI omenta, CD138<sup>+</sup>Blimp1-tdTomato<sup>+</sup> KI PC were mostly observed surrounding B220<sup>+</sup> FALCs, and PC were rarely detected in control omenta (**Figure 2.4 C**).

### **Stromal PLA1A is required for PerC KI PC and MemB maintenance**

To test the ligand-dependence of KI cell accumulation in the PerC, we co-transferred control and KI PerC cells via IP injection into PLA1A-sufficient and -deficient recipient mice (**Figure 2.5 A**). At 7 days, there was decreased recovery of donor KI PC and MemB from

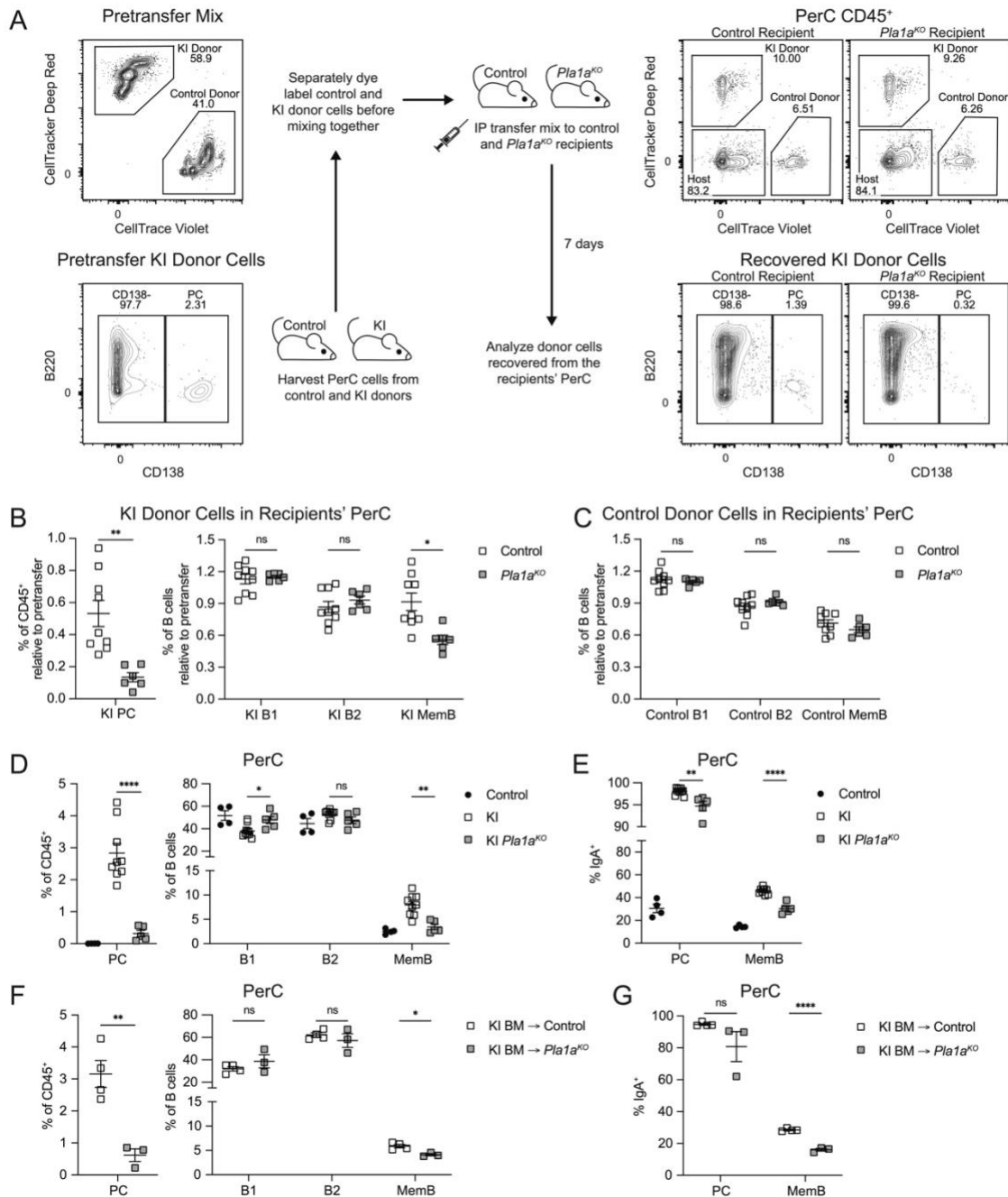


**Figure 2.5. GPR34 KI PerC PC and MemB maintenance depends on stromal PLA1A.**

(A-G) PerC immune cells were analyzed by flow cytometry. (A-C) PerC cells from control and KI (*Cd21<sup>Cre</sup>R26<sup>LSL-Gpr34Q340X-IRES-GFP</sup>*) mice were dye labeled, mixed, and IP transferred into control (*Pla1a<sup>WT</sup>* or *Het*) or *Pla1a<sup>KO</sup>* recipient mice, whose PerC cells were analyzed on day 7. (A) Left top: Representative flow cytometry plot of pretransfer mix gated for dye labeled donor cells. Left bottom: Representative flow cytometry plot of pretransfer KI donor cells gated for PC (CD138<sup>+</sup>) and annotated with PC frequency. Middle: Schematic of IP adoptive transfer experiment. Right top: Representative flow cytometry plots of recipient PerC CD45<sup>+</sup> cells gated for donor cells. Right bottom: Representative flow cytometry plots of recovered KI donor cells (Figure caption continued on the next page.)

(Figure caption continued from the previous page.)

gated for PC and annotated with PC frequency. **(B and C)** Plots show the frequencies of recovered co-transferred PC, B1 (IgD<sup>+</sup>IgM<sup>+</sup>), B2 (IgD<sup>+</sup>IgM<sup>+</sup>), and MemB (IgD<sup>+</sup>IgM<sup>-</sup>) normalized to their respective pretransfer frequencies (control,  $n = 9$ ; *Plala*<sup>KO</sup>,  $n = 6$ ). **(D)** Frequencies of the indicated populations in control mice and in KI mice on either a control or *Plala*<sup>KO</sup> background (control,  $n = 4$ ; KI,  $n = 9$ ; KI *Plala*<sup>KO</sup>,  $n = 5$ ). **(E)** Frequencies of IgA<sup>+</sup> cells within the indicated populations (control,  $n = 4$ ; KI,  $n = 9$ ; KI *Plala*<sup>KO</sup>,  $n = 5$ ). **(F)** Frequencies of the indicated populations in chimeric mice with KI BM reconstituted into control or *Plala*<sup>KO</sup> hosts (control,  $n = 4$ ; *Plala*<sup>KO</sup>,  $n = 3$ ). **(G)** Frequencies of IgA<sup>+</sup> cells within the indicated populations (control,  $n = 4$ ; *Plala*<sup>KO</sup>,  $n = 3$ ). Each data point represents an individual mouse, lines indicate means, and error bars represent SEM. Data were pooled from three (B and C) or two (D-G) independent experiments. Statistical significance (B-G) was determined by unpaired *t* test corrected for multiple comparisons (Holm-Šidák). ns, not significant; \* $P < 0.05$ ; \*\* $P < 0.01$ ; \*\*\*\* $P < 0.0001$ .

*Plala*<sup>KO</sup> recipients compared with controls (**Figure 2.5, A and B**). Recovery of donor control MemB was unaffected, as was the recovery of other populations (**Figure 2.5 C**). These results indicate that KI PC maintenance is PLA1A-dependent, and that KI MemB maintenance is both PLA1A-dependent and GPR34-dependent. To obtain sufficient control PC for comparison to their KI counterparts, we IP co-transferred an equal mixture of control and KI spleen cells into WT mice. At 7 days, there was much greater recovery of donor KI PC than control PC, while B cells as a whole were unaffected (**Supplementary Figure 2.3 E**). Thus, KI PC maintenance in the PerC is also GPR34-dependent.

Next, we studied the PLA1A dependence of PerC KI PC and MemB by intercrossing KI and *Plala*<sup>KO</sup> mice. KI mice lacking the *Plala* gene showed an almost complete block in PerC accumulation of KI PC and MemB (**Figure 2.5 D**). The increased IgA positivity of KI PC and MemB was also partially dependent on PLA1A (**Figure 2.5 E**). However, enzyme deficiency had minimal effect on the Ki67<sup>+</sup> frequency of KI MemB (**Supplementary Figure 2.3 F**), and amongst the PC remaining in the PerC of these mice, the Ki67<sup>+</sup> fraction was elevated. These data suggest that in contrast to the effect on cell accumulation, KI MemB proliferation in the PerC does not require a ligand generated by PLA1A. To determine the contribution of stromal PLA1A to KI cell accumulation, we made BM chimeras in which we reconstituted PLA1A-deficient or control hosts with KI BM. In the *Plala*<sup>KO</sup> hosts, enzyme expression is lacking in the stromal compartment but intact in the hematopoietic system. The KI PC and MemB frequencies were reduced in *Plala*<sup>KO</sup> hosts (**Figure 2.5 F**), signifying a substantial dependence on stroma-derived lysoPS. Stromal PLA1A also contributed to the enrichment of KI IgA<sup>+</sup> cells (**Figure 2.5 G**). Non-KI PC and MemB were not affected by PLA1A deficiency (**Supplementary Figure 2.3 G**).

## Concluding remarks

Our work reveals that GPR34 can drive the ligand-dependent accumulation of immune cells in the PerC. Immune cell homing is guided by many inputs, and it is likely that GPR34 cooperates with other factors to enable preferential PerC localization. Although with a smaller effect size, the GPR34 GOF allele also promoted PC accumulation in the PleuralC. Prior in vitro studies showed that *sn*-2 lysoPS is the more potent and likely physiological form of GPR34 ligand (Kitamura et al., 2012; Uwamizu et al., 2015; Izume et al., 2024), but the in vivo relevance of PLA1A-generated lysoPS has been elusive. The serendipitous discovery of GPR34 KI-mediated PerC PC and MemB accumulation allowed us to probe this enzyme-ligand-receptor axis. Omental *sn*-2 lysoPS levels and PerC KI cell maintenance depended on PLA1A, supporting a model where stromal cells regulate lipid mediators that govern immune cell residence. Further study is needed to understand the spatial distribution of *sn*-2 lysoPS and thus its availability to GPR34-expressing cells. The substrate of PLA1A is PS, and the relevant source of PS in the omentum at homeostasis remains unclear. Since PLA1A can generate lysoPS from PS that is externalized to the outer leaflet of dying cells (Hosono et al., 2001), we speculate that a homeostatic level of cell death may provide sufficient substrate. Alternatively, cell death may not be required at all, as viable cells can also externalize PS (Zhao et al., 2021; Segawa et al., 2011; Elliott et al., 2005).

At the receptor level, GPR34 KI can promote cell cycle activation as well as ex vivo migration of B-lineage lymphocytes, but further investigation will be needed to establish whether GPR34 mediates migration in vivo. We speculate that the PerC accumulation of KI PC and MemB involves cell recruitment from circulation or possibly through lymphatics or even across the visceral peritoneal linings of PerC organs. Cell proliferation within the PerC then further

contributes to PC and MemB abundance. It is also possible that some PerC PC are derived from local MemB rather than traveling from the PP. The proposed cell recruitment step likely occurs at a low rate, making it problematic to detect using conventional adoptive transfer approaches and requiring the generation of new methods for its study. Although we favor a role for GPR34 in promoting migration to the PerC, our data are also consistent with the receptor promoting retention of cells already inhabiting the PerC. Our finding that the pro-proliferative activity of GPR34 in PerC MemB was not dependent on PLA1A may be explained by the GOF receptor having sufficient constitutive activity to engage proliferative pathways in these cells or by the existence of PLA1A-independent ligands (such as *sn*-1 forms of lysoPS) in the PerC.

Although we did not observe SG KI cell accumulation or lymphoma in our mouse model (even in mice aged over 6 months, unpublished data), we hypothesize that GPR34 GOF-driven proliferation and migration contribute to the eventual development of SG MALT lymphomas in a Sjogren's syndrome context (Korona et al., 2021; Pringle et al., 2022). Autoimmune inflammation could potentially boost PLA1A expression in the SG, and cell death in lymphoepithelial lesions would increase the availability of PS substrate that can be converted to lysoPS. In addition, we speculate that GPR34 cooperates with other factors in promoting KI cell localization in the PerC and that those cooperating factors may be lacking in the uninflamed SG. Intriguingly, PC have been observed in up to one-third of SG MALT lymphomas (Molina et al., 2011) as well as in MALT lymphomas more generally, with occasional cases where PC constitute >80% of an extranodal tumor's total cellularity (Wöhrer et al., 2007). The expansion of PerC PC in our model also echoes rare PerC plasmacytomas in patients (Thambi et al., 2018), including cases specifically associated with the omentum (Peison et al., 1980; Soliman et al., 2019). It remains unknown whether GPR34 plays a role in the PerC localization of PC

malignancy. Finally, although we did not identify an effect of GPR34 deficiency on MemB or PC abundance in the PerC in our immunization studies, it remains possible that there exist physiologic conditions where they home to or accumulate in the PerC in a GPR34-dependent manner. Overall, this work connects PLA1A and GPR34 biology to define a ligand-receptor system that has the capacity to promote cell compartmentalization in the PerC.

## **SUPPLEMENTARY FIGURES**

Supplementary Figure 2.1.

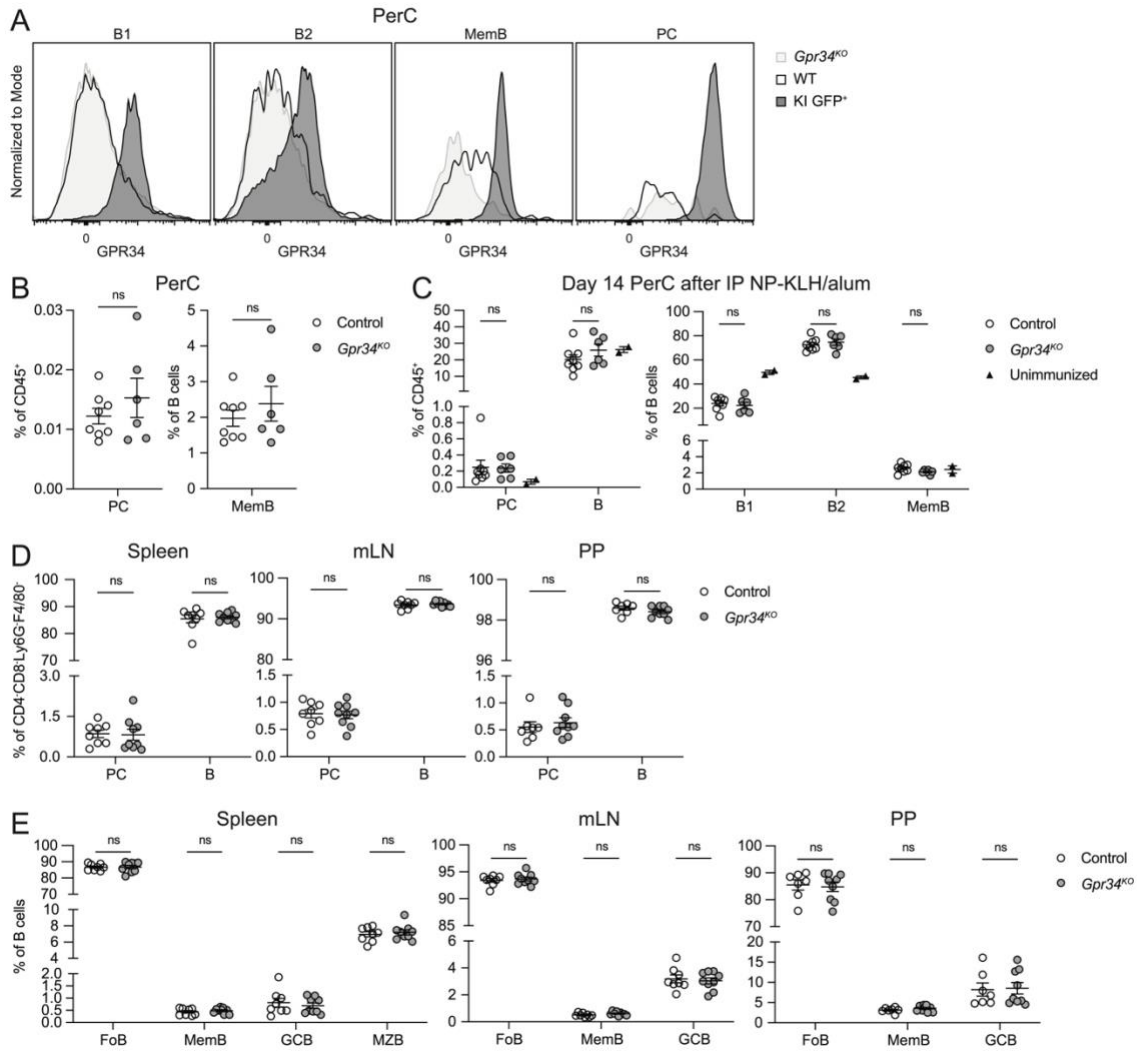
Supplementary Figure 2.2.

Supplementary Figure 2.3.



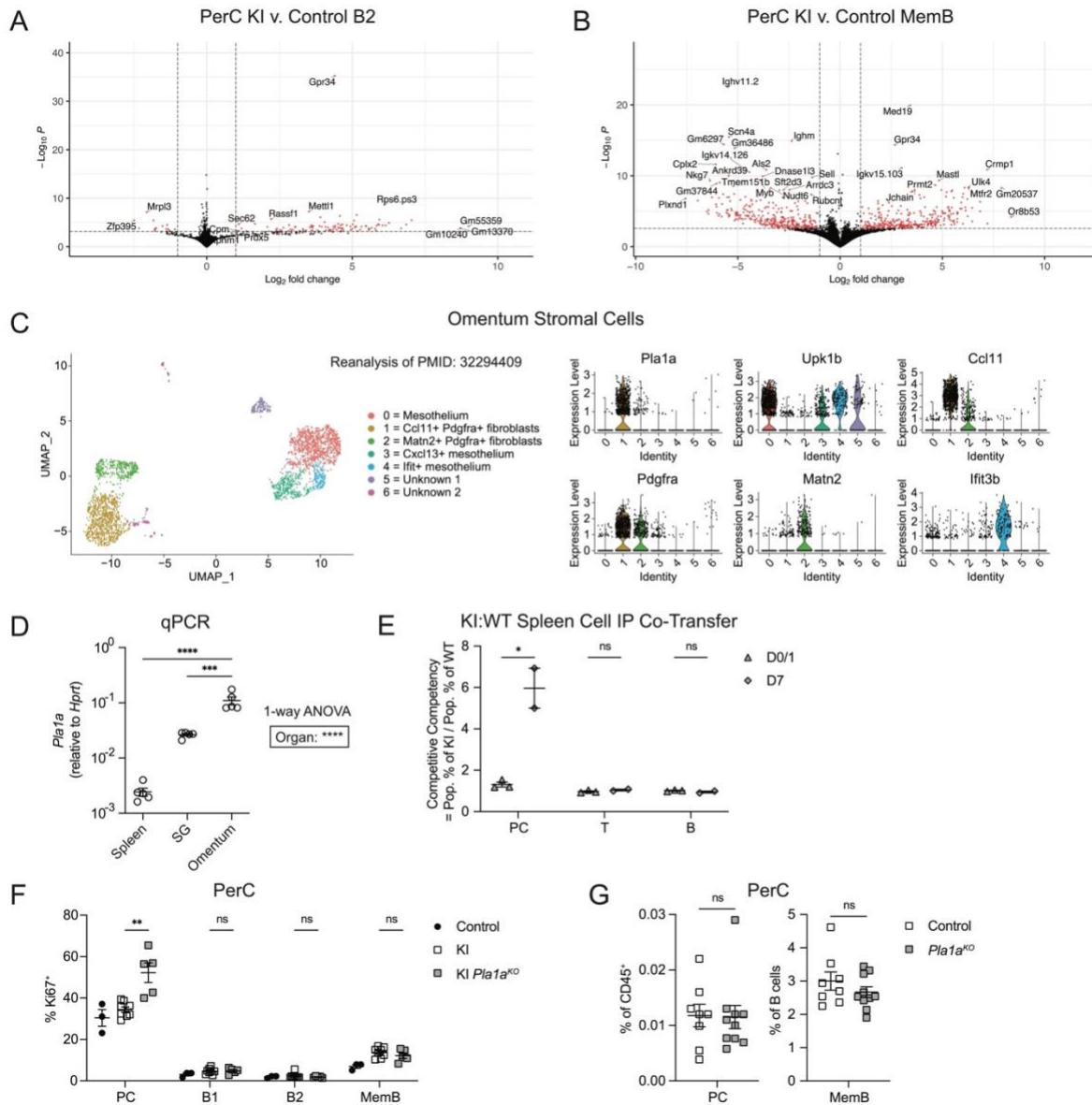
(Figure caption continued from the previous page.)

gated for GFP reporter expression and annotated with GFP<sup>+</sup> percentage. **(D)** Cell numbers of B cells from the spleen, iLN, and SG of control and KI mice (spleen,  $n = 12$ ; iLN,  $n = 4$ ; SG,  $n = 7$ ). **(E)** Frequencies of PerC PC (CD138<sup>+</sup>), B1 (IgD<sup>-</sup>IgM<sup>+</sup>), B2 (IgD<sup>+</sup>IgM<sup>+</sup>), and MemB (IgD<sup>-</sup>IgM<sup>-</sup>) in chimeric mice with control or KI BM reconstituted into WT hosts (control,  $n = 6$ ; KI,  $n = 6$ ). **(F)** Representative flow cytometry histograms of CCR9 expression in the indicated PerC populations. **(G-J)** Data for iLN, cLN, and liver each include 3 BM chimeric mice. PC were gated as B220-IgA<sup>+</sup> in the SI LP and CD138<sup>+</sup> otherwise. MemB were gated as IgD<sup>-</sup>IgM<sup>-</sup> in the PerC, IgD<sup>-</sup>IgM<sup>-</sup>CD38<sup>+</sup>GL7<sup>-</sup> in the BM, and IgD<sup>-</sup>CD38<sup>+</sup>GL7<sup>-</sup>CD95<sup>+</sup> otherwise. **(G)** Frequencies of IgA<sup>+</sup> cells within PC and MemB in the indicated organs (control PerC PC,  $n = 7$ ; other PerC,  $n = 16-17$ ; spleen,  $n = 9-11$ ; mLN,  $n = 9-10$ ; PP,  $n = 9$ ; iLN,  $n = 5$ ; cLN,  $n = 5$ ; liver,  $n = 3$ ; BM,  $n = 2$ ; PleuralC,  $n = 5-8$ ). **(H and I)** Frequencies of PC and MemB in the indicated organs (PerC,  $n = 14-15$ ; spleen,  $n = 14$ ; mLN,  $n = 13-14$ ; PP,  $n = 11$ ; iLN,  $n = 7$ ; cLN,  $n = 9$ ; liver,  $n = 3$ ; BM,  $n = 6$ ; PleuralC,  $n = 6-8$ ; SI LP,  $n = 5$ ). **(J)** Frequencies of GFP<sup>+</sup> cells within PC and MemB in the indicated organs (PerC,  $n = 17$ ; spleen,  $n = 13$ ; mLN,  $n = 12$ ; PP,  $n = 11$ ; iLN,  $n = 7$ ; cLN,  $n = 8$ ; liver,  $n = 3$ ; BM,  $n = 5$ ; PleuralC,  $n = 6$ , SI LP,  $n = 5$ ). Each data point represents an individual transwell (A) or mouse (D, E, and G-J), lines indicate means, and error bars represent SEM. Data were pooled from three or more independent experiments, except in D and G, which were pooled from two or more independent experiments. Statistical significance (D, E, and G-J) was determined by unpaired  $t$  test corrected for multiple comparisons (Holm-Šidák). ns, not significant; \* $P < 0.05$ ; \*\* $P < 0.01$ ; \*\*\* $P < 0.001$ ; \*\*\*\* $P < 0.0001$ .



### Supplementary Figure 2.2. GPR34 deficiency does not result in PC or B cell accumulation defects.

(A) Representative flow cytometry histograms of polyclonal anti-GPR34 antibody surface staining of the indicated PerC populations from *Gpr34*<sup>KO</sup>, WT, and KI (*Cd21*<sup>Cre</sup>*R26*<sup>LSL</sup>-*Gpr34*<sup>Q340X</sup>-*IRE5*-*GFP*) mice. (B-E) Immune cells from control and *Gpr34*<sup>KO</sup> mice were analyzed by flow cytometry. (B) Frequencies of PC (CD138<sup>+</sup>) and MemB (IgD<sup>-</sup>IgM<sup>-</sup>) in the PerC (control, *n* = 8; *Gpr34*<sup>KO</sup>, *n* = 6). (C) Frequencies of PC, B, B1 (IgD<sup>-</sup>IgM<sup>+</sup>), B2 (IgD<sup>+</sup>IgM<sup>+</sup>), and MemB in the PerC fourteen days after mice were immunized IP with NP-KLH in alum adjuvant or left unimmunized (control, *n* = 8; *Gpr34*<sup>KO</sup>, *n* = 6; unimmunized, *n* = 2). (D and E) Frequencies of PC, B, FoB (IgD<sup>+</sup>CD38<sup>+</sup>), MemB (IgD<sup>-</sup>CD38<sup>+</sup>GL7<sup>-</sup>CD95<sup>+</sup>), GCB (IgD<sup>-</sup>CD38<sup>-</sup>GL7<sup>+</sup>CD95<sup>+</sup>), and MZB (IgD<sup>int</sup>CD38<sup>hi</sup>) in the indicated organs (control, *n* = 7-8; *Gpr34*<sup>KO</sup>, *n* = 9). Each data point represents an individual mouse (B-E), lines indicate means, and error bars represent SEM. Data were pooled from two independent experiments. Statistical significance (B-E) was determined by unpaired *t* test corrected for multiple comparisons (Holm-Šidák). ns, not significant.



**Supplementary Figure 2.3. GPR34 KI alters gene expression of PerC cells, omental fibroblasts express PLA1A, and GPR34 KI supports PC maintenance in the PerC.** (A and B) B2 (IgD<sup>+</sup>IgM<sup>+</sup>) and MemB (IgD<sup>+</sup>IgM<sup>-</sup>) cells were sorted from the PerC from control and KI mice for bulk RNA sequencing (control B2,  $n = 3$ ; control MemB,  $n = 3$ ; KI B2,  $n = 3$ ; KI MemB,  $n = 3$ ). Volcano plots display in red the DEGs with a  $\log_2$  fold change  $>1$  and an adjusted  $P < 0.05$  for the indicated comparisons. (C) Seurat reanalysis of the mouse omental stromal cell single cell RNA sequencing dataset from Jackson-Jones et al. (2020). Violin plots show normalized expression of *Pla1a* and cluster-defining markers. (D) qPCR for expression of *Pla1a* (relative to *Hprt*) in whole spleen, SG, and omentum tissues from WT mice (spleen,  $n = 5$ ; SG,  $n = 5$ ; omentum,  $n = 5$ ). (E-G) Immune cells were analyzed by flow cytometry. (E) Spleen cells from control and KI (*Cd21<sup>Cre</sup>R26<sup>LSL</sup>-Gpr34<sup>Q340X</sup>-IRES-GFP*) mice were harvested, dye-labeled, mixed, and co-transferred IP into congenic recipients. Donor cell recovery from recipients' PerC was analyzed by flow cytometry for PC (CD138<sup>+</sup>), T cells (TCRb<sup>+</sup>), and B cells (CD19<sup>+</sup>) on the (Figure caption continued on the next page.)

(Figure caption continued from the previous page.)

indicated days after transfer. For a given population, the competitive competency is defined as the ratio between its frequency among KI cells and its frequency among control cells, which reflects the multiplicity of the numerical advantage of KI over control. **(F)** Frequencies of Ki67<sup>+</sup> cells within the indicated PerC populations from control, KI, and KI *Plal*<sup>KO</sup> mice (control, *n* = 4; KI, *n* = 9; KI *Plal*<sup>KO</sup>, *n* = 5). **(G)** Frequencies of the indicated PerC populations in control (*Plal*<sup>WT</sup> or <sup>Het</sup>) and *Plal*<sup>KO</sup> mice (control, *n* = 8; *Plal*<sup>KO</sup>, *n* = 10). Each data point represents an individual mouse (D-G), lines indicate means, and error bars represent SEM. In D-G, data were pooled from two independent experiments, except in E, which was from one experiment. Related to E, similar findings were obtained in separate groups of recipient mice that received donor mLN and PP cells. Statistical significance was determined by one-way ANOVA, followed by paired *t* test of each tissue to the omentum corrected for multiple comparisons (Holm-Šídák) (D) or by unpaired *t* test corrected for multiple comparisons (Holm-Šídák) (E-G). ns, not significant; \**P* < 0.05; \*\**P* < 0.01; \*\*\**P* < 0.001; \*\*\*\**P* < 0.0001.

## MATERIALS AND METHODS

### Mice

*R26<sup>LSL-Gpr34Q340X-IRES-GFP</sup>* mice were generated on a C56BL/6N background by CRISPR/Cas9-mediated targeting of and homologous recombination at the *Rosa26* locus (Biocytogen Boston Corp.), resulting in the conditional KI allele shown in **Figure 2.1 A**. *Plal1a<sup>KO</sup>* (*Plal1a<sup>tm1a(EUCOMM)Wtsi</sup>*) mice were generated from ES cells of a C56BL/6N background purchased from EUCOMM. *Cd21<sup>Cre</sup>* (Kraus et al., 2004), *Gpr34<sup>KO</sup>* (Liebscher et al., 2011), *Blimp1<sup>CreERT2</sup>* (Robinson et al., 2023), and *Em-bcl2* (Strasser et al., 1991) mice have been described previously. *Blimp1<sup>CreERT2</sup>* mice were provided by D. Tarlinton (Monash University, Melbourne, Australia). Mice were analyzed at 8-20 wk of age. Congenic hosts for BM chimeras and recipients for transfer experiments were either B6 CD45.1 (002014) mice bred internally from founders ordered from The Jackson Laboratory or B6-Ly5.1/Cr (564) mice purchased from the National Cancer Institute at Charles River at age 6-8 wk. To produce BM chimeric mice, hosts were lethally irradiated with 900 cGy X-ray irradiation (split dose separated by 3 h), followed by IV injection of BM cells from donors. Chimeras were analyzed for donor-derived immune cells 8-12 wk after reconstitution. Mice were co-caged with littermates for all experiments. All data are representative of male and female mice. Control and experimental treatments were administered to age- and sex-matched mice that had been allocated to groups randomly, with sample sizes chosen based on previous experience. The investigators were not blinded. Animals were housed in a specific pathogen-free environment in the Laboratory Animal Research Center at the University of California, San Francisco (UCSF), and all experiments conformed to ethical principles and guidelines approved by the UCSF Institutional Animal Care and Use Committee.

## **Treatments and immunizations**

For conditional activation of *Blimp1*<sup>CreERT2</sup>, 6 mg tamoxifen (Sigma-Aldrich) was administered via oral gavage on days 0 and 1 (Robinson et al., 2023). Mice were analyzed at various timepoints thereafter. For labeling of proliferating cells, mice were IP-injected with 0.5 mg of EdU (Thermo Fisher Scientific) 90 min before analysis. To induce a PerC PC response, mice were immunized IP with 100 µg NP30-KLH (Biosearch Technologies) in 2% Alhydrogel alum adjuvant (Invivogen).

## **Cell preparation**

Peritoneal and pleural lavage cells were isolated by flushing the PerC and PleuralC with 5 or 1 ml of MACS buffer (PBS containing 2% newborn calf serum [NBCS] and 1 mM EDTA), respectively. To collect cells physically associated with the visceral peritoneal surface of tissues, mice were transcardially perfused with PBS to reduce blood contamination before the PerC was opened. PerC organs were harvested and rinsed in 5 ml MACS, and the MACS rinse media was analyzed. Cell suspensions were prepared from the spleen, iLN, mLN, PP, and cLN by gentle mashing through a 70-µm strainer. The liver was mashed through a 100-µm strainer and purified for immune cells by resuspending in 40% Percoll (Thermo Fisher Scientific) and centrifuging at 2,500 rpm for 20 min at room temperature on low brake. The immune cell pellet was collected from the bottom of the tube. BM cells from leg bones were extracted by centrifugation in a microfuge at 10,000 rpm for 3 min at 4°C. To generate SG immune cell suspensions, the submandibular and sublingual glands were dissected and minced using scissors. The minced SG tissue was then incubated for 30 min shaking (1,000 rpm) at 37°C in 1 ml of RPMI with 2% NBCS, 10 mM HEPES, 1 mg/ml collagenase type IV (Worthington), and 20 µg/ml DNase I

(Sigma-Aldrich). To stop the digestion, 20  $\mu$ l of 500 mM EDTA was added to each sample. The digested SG tissue was mashed through a 100- $\mu$ m strainer, washed with MACS buffer, and purified for immune cells using 40% Percoll. To prepare SI LP samples, PP and intestinal contents were removed from the SI, and the first 12 cm (duodenum) were cut into several pieces for further processing. The SI tissue was twice incubated for 20 min shaking (250 rpm) at 37°C in 12 ml of intraepithelial lymphocyte media (HBSS containing 5% FBS, 2 mM EDTA, and 1 mM dithiothreitol [Sigma-Aldrich]). The intraepithelial lymphocyte fractions were discarded. The tissue was then twice digested for 20 min in 12 ml of LP media (RPMI containing 10% FBS, 100  $\mu$ g/ml DNase I, and 0.232 mg/ml collagenase VIII from *Clostridium histolyticum* [Sigma-Aldrich]). The two LP fractions were aggregated and purified using 40% Percoll.

### **Adoptive transfer experiments**

For IV transfers, PerC, spleen, mLN, and PP cell suspensions were prepared from congenically marked control and KI donor mice. These cells were transferred IV via retroorbital injection into congenically marked recipient mice, whose PerC and spleen were analyzed after 3 days for quantification of donor cells.

For IP transfers, donor control and KI PerC cells were dye labeled with CellTrace Violet (Invitrogen) and CellTracker Deep Red (Invitrogen), respectively. These cells were then co-transferred via IP injection into control or *Plala<sup>KO</sup>* mice. In one experiment, donor control and KI spleen cells were similarly dye-labeled and co-transferred IP into congenic WT mice. Recipients' PerC were analyzed for donor cell maintenance after 7 days.

## Flow cytometry

Cells were washed, blocked with 2.4G2 antibody (Bio X Cell), and stained for 30 min on ice in MACS buffer. The following antibodies were used: CD11b-BUV496 (BD), CD19-BUV563 (BD), IgM-BUV661 (BD), TCRb-BUV737 (BD), CD138-BV421 (Biolegend), CD45.2-BV421 (Biolegend), CD21/35-PB (Biolegend), GL7-PB (Biolegend), B220-BV510 (Biolegend), CD11b-BV570 (Biolegend), CD19-BV605 (Biolegend), CD45.1-BV605 (Biolegend), CD45.2-BV605 (Biolegend), IgD-BV650 (Biolegend), CD45.1-BV650 (Biolegend), CD138-BV711 (Biolegend), IgD-BV711 (Biolegend), CD98-BV711 (BD), EpCAM-BV711 (Biolegend), CD95-BV750 (BD), CD11b-BV785 (Biolegend), CD138-BV785 (Biolegend), CD45.1-BV785 (Biolegend), CD95-BV786 (BD), CD45-AF532 (Invitrogen), CD21/35-PE (BD), CD23-PE (BD), GL7-PE (eBioscience), IgA-PE (Southern Biotech), CD45.2-PE (Biolegend), CD23-PE/Cy7 (Biolegend), CD38-PE/Cy7 (Biolegend), IgM-PE/Cy7 (eBioscience), CD45.1-PE/Cy7 (eBioscience), IgM-PerCP/Cy5.5 (Biolegend), GL7-PerCP/Cy5.5 (Biolegend), CD45.2-PerCP/Cy5.5 (Tonbo), CD38-BB700 (BD), CCR9-APC (eBioscience), CD45.1-APC (Cytex), CD21/35-AF647 (Biolegend), CD38-AF647 (Biolegend), CD45.2-AF647 (Biolegend), GL7-AF647 (Biolegend), B220-AF700 (Biolegend), CD38-AF700 (eBioscience), CD45.1-AF700 (Biolegend), CD45.2-AF700 (Biolegend), CD4-APC/Cy7 (Cytex), CD8a-APC/Cy7 (Cytex), Ly6G-APC/Cy7 (Cytex), F4/80-APC/Cy7 (Biolegend), B220-APC/Fire810 (Biolegend), and IgA-biotin (Southern Biotech) (followed by streptavidin-BV605 [Biolegend] or streptavidin-BV711 [BD]). Dead cells were excluded using Fixable Viability Dye eFluor780 (eBioscience).

For Ki67 detection, cells were stained with surface antibodies, pre-fixed with 1% paraformaldehyde in PBS for 10 min on ice, and fixed and permeabilized with the

Foxp3/Transcription Factor Staining Buffer Set (eBioscience), before intracellular staining with the Ki67-AF647 antibody (BD). For detection of EdU incorporation, the Click-iT Plus EdU Flow Cytometry Assay Kit (Invitrogen) was used. GPR34 surface staining was enabled by a polyclonal rabbit antibody raised against the first 40 N-terminal amino acids of mouse GPR34 (Biomatik). The polyclonal reagent was cross-absorbed on a *Gpr34<sup>KO</sup>* spleen cell suspension overnight to reduce non-specific binding. After blocking, WT and KI cells were stained with the polyclonal rabbit anti-GPR34 antibody for 1 h at room temperature, followed by donkey anti-rabbit biotin-SP (Jackson Immunoresearch) for 20 min on ice, and finally SA-AF647 (Invitrogen) and other surface markers for 30 min on ice.

All samples were run on a Cytex Aurora. Flow cytometry data were analyzed using FlowJo (v10.10.0).

### **Cell sorting and RNA sequencing**

B2 (IgD<sup>+</sup>IgM<sup>+</sup>) and MemB (IgD<sup>-</sup>IgM<sup>-</sup>) cells were sorted from the PerC of control and KI mice using a BD FACSAria II. Sort purity was ~95%. The sequencing library was prepared using Ovation RNA-seq System V2 from Nugen, the KAPA Hyper prep labeling kit, and the NEXTflex DNA barcodes Adapter kit from Bioo Scientific. 50 bp paired-end reads were acquired on a NovaSeq X at the UCSF Center for Advanced Technology. FastQC was used to examine the quality of raw sequencing reads, and cutadapt was used to trim adaptors and clean reads. Sequences were aligned to the mm39 genome with STAR, followed by quantification with RSEM, PCA with pcaExplorer, and differential gene expression analysis with DEseq2. Cutoffs for DEGs were set at a log<sub>2</sub> fold change >1 and an adjusted P < 0.05. DEGs between KI and control were subjected to GO analysis (<https://geneontology.org/>). The PCA plot was generated

by pcaExplorer. The heatmap was generated with pheatmap. Volcano plots were generated with EnhancedVolcano.

### **Published scRNAseq data analysis**

The Seurat R package (<https://satijalab.org/seurat/>) was used to reanalyze an omental stromal cell scRNAseq dataset (Jackson-Jones et al., 2020).

### **Generation of GPR34-expressing WEHI-231 cells**

Mouse *Gpr34* or *Gpr34R337X* was cloned into the pQEF retroviral vector (Yang and Allen, 2018) followed by a P2A-Thy1.1 as an expression marker. Retrovirus was generated by transfecting the Plat-E packaging cell line with 1.5 µg plasmid DNA and 3 µL Lipofectamine 2000 (Life Technologies). WEHI-231 mouse B lymphoma cells were grown in RPMI containing 10% FBS, 10 mM HEPES, 2 mM glutamine, 55 µM 2-mercaptoethanol, and 50 U penicillin/streptomycin.  $5 \times 10^5$  WEHI-231 cells were placed in a well of a 6-well plate along with the retroviral supernatant. The cells were centrifuged at 2,400 rpm for 2 h at 32°C. This spinfection was repeated with fresh retrovirus 24 h later. After 1 wk, Thy1.1-expressing cells were sorted using a BD FACSAria II.

### **Transwell migration assays**

WEHI-231 cells were taken from T25 flask cultures and washed twice in prewarmed migration media (RPMI containing 0.5% fatty acid-free BSA, 10 mM HEPES, and 50 U penicillin/streptomycin). PerC cells, obtained from peritoneal lavage using migration media, were washed once. Both WEHI-231 and PerC cells were resuspended at  $1 \times 10^7$  cells per mL and

resensitized for 10 min in a 37°C water bath. 100 µl of cells ( $1 \times 10^6$  cells) were added on top of transwells (5-µm pore, Corning) with CXCL13 (Thermo Fisher Scientific), CCL25 (Biolegend), or lysoPS 18:1 (Avanti Polar Lipids) in migration media (600 µl) in the bottom chamber. The cells were allowed to migrate for 3 h, after which the cells in the bottom well were analyzed and counted by flow cytometry.

### **Immunofluorescence staining and microscopy**

Mice were IP-injected with 1 µg each of CD138-BV421 (Biolegend) and B220-AF647 (Biolegend) 30 min before analysis. Omenta were carefully harvested, gently dipped once in PBS, and whole-mounted fresh on Superfrost Plus microscope slides (Thermo Fisher Scientific). Images were immediately acquired with a HP PL FLUOTAR 10X/0.2 AIR objective on a Stellaris DIVE confocal microscope (Leica) using LAS X software (Leica) and subsequently processed using ImageJ (v2.14.0).

### **LC-MS/MS**

To distinguish and quantify the *sn*-1 and *sn*-2 forms of lysoPS, we adapted an established LC-MS/MS protocol (Okudaira et al., 2014). Omenta were harvested, weighed, and immediately added to Precellys 0.5 mL soft tissue homogenizing tubes (Cayman Chemicals) containing 9 vol (relative to omentum weight) of ice-cold acidic methanol (pH 4.0) with 50 nM lysoPS 17:1 (Avanti Polar Lipids) internal standard. Samples were homogenized using a Precellys 24 homogenizer with a Cryolys cooling unit (Bertin Technologies). The homogenization program consisted of three cycles for 20 s at 6,400 rpm (with 30 s breaks) at a temperature <4 °C. Lysate was recovered, the homogenizing tube was washed with 10 vol (relative to omentum weight) of

acidic methanol, and the wash was combined with the lysate before centrifuging at 21,000 rpm for 10 min at 4°C. 50 µl of supernatant was concentrated by drying in a DNA Speed Vac for 20 min. Samples were resuspended in 15 µl acidic methanol and centrifuged at 21,000 rpm for 10 min at 4°C. 10 µl supernatant was transferred to glass vials with 9 mm autosampler inserts.

Samples were analyzed using a SCIEX ExionLC UPLC in series with a SCIEX QTRAP 7500. 5 µl of each sample was injected and separated using a 5 µm CAPCELL PAK C18 column (150mm × 1.5mm; Shiseido). The mobile phase scheme consisted of A (5 mM ammonium formate in H<sub>2</sub>O, pH 4.0) and B (5 mM ammonium formate in 95% [vol/vol] acetonitrile, pH 4.0) delivered at a flow rate of 0.250 ml/min. Analytes were separated using the following gradient: 55% B (initial), 55% B (10 min), 85% B (30 min), 85% B (37 min), 55% B (37.1 min), and 55% B (45 min). Data were acquired in negative mode using the transitions (*m/z*) 524.3 → 437.3, 522.3 → 435.3, 544.3 → 457.2, and 508.3 → 421.3 for 18:0 lysoPS, 18:1 lysoPS, 20:4 lysoPS, and 17:1 lysoPS (as an internal standard), respectively. The ion source temperature was maintained at 350°C. The spraying needle voltage was at -2 kV. Gas 1, gas 2, curtain gas, and collision gas were set at 60, 40, 40, and 9 respectively. The entrance potential was set at -10 V, and the collision exit potential was -15 V. Collision energy was -22 eV for all compounds. Peak areas were determined using SCIEX OS. Analyte abundance was quantified as the peak area ratio, defined as the peak area of the analyte divided by the peak area of the internal standard.

### **Quantitative PCR**

Total RNA from homogenized spleen, SG, and omentum was extracted using an RNeasy kit (Qiagen) and reverse-transcribed using M-MLV reverse transcriptase (Invitrogen). qPCR was performed using Power SYBR Green (Applied Biosystems) with an Applied Biosystems

StepOnePlus instrument. Data were analyzed with the comparative Ct ( $2^{-\Delta\Delta C_t}$ ) method, using *Hprt* as a housekeeping gene. The following primers were used: Pla1a, (F) 5'-TGGAGTTTTATTTGAAGGAGA-3' and (R) 5'-GTGGGTTAGGATGAGCCAT-3'.

### **Statistical analyses**

Data were analyzed using unpaired or paired *t* tests corrected for multiple comparisons (Holm-Šídák), repeated measures one-way ANOVA, or two-way ANOVA as specified in the figure legends. Prism software (GraphPad v10.2.3) was used for all statistical analyses and to generate plots. Each experiment was repeated at least three times unless otherwise indicated in the figure legends. In summary graphs, points indicate individual samples, horizontal lines are means and error bars represent SEM. Levels of significance were defined as \**P* < 0.05, \*\**P* < 0.01, \*\*\**P* < 0.001, and \*\*\*\**P* < 0.0001.

## DATA AVAILABILITY

Bulk RNA-seq data from this study have been deposited to Gene Expression Omnibus (GEO) (accession GSE274652). The reanalyzed scRNAseq dataset (Jackson-Jones et al., 2020) in **Supplementary Figure 2.3 C** is openly available in GEO (accession GSM4053741). All other data are available in the article itself and its supplementary materials and are also available upon request from the corresponding author.

## ACKNOWLEDGEMENTS

We thank David Tarlinton (Monash University, Melbourne, Australia) for *Blimp1<sup>CreERT2</sup>* mice and Cliff Lowell and Nikhita Kirthivasan for their comments on the manuscript.

Sequencing was performed at the UCSF Center for Advanced Technology, supported by the UCSF Program for Breakthrough Biomedical Research, Research Resource Program Institutional Matching Instrumentation Awards, and National Institutes of Health (NIH) 1S10OD028511-01 grants. Cell sorting was performed at the UCSF Parnassus Flow Cytometry CoLab, supported in part by NIH grant P30 DK063720 and by the NIH S10 instrumentation grant S10 1S10OD021822-01. H. Tam was supported by the NIH-funded UCSF Medical Scientist Training Program (T32GM141323) and is now supported by NIH F30 grant F30CA284515. J.G. Cyster is an investigator of the Howard Hughes Medical Institute. This work was supported in part by NIH grant R01 AI045073.

Disclosures: J.G. Cyster reported personal fees from BeBio Pharma, personal fees from Lycia Therapeutics, and personal fees from DrenBio Inc. outside the submitted work. No other disclosures were reported.

## **CHAPTER 3**

### **Conclusion**

## Conclusion

In this study, we reveal that GPR34 can promote the ligand-dependent accumulation of immune cells in the PerC. Despite *in vitro* and structural reports indicating that *sn*-2 lysoPS is the more potent and likely physiological form of GPR34 ligand (Kitamura et al., 2012; Uwamizu et al., 2015; Izume et al., 2024), the *in vivo* relevance of PLA1A-generated lysoPS has not been previously demonstrated. Indeed, recent publications on GPR34's role in microglia and type 1 innate lymphoid cells identified ABHD16A as the lysoPS-producing enzyme and did not distinguish *sn*-1 versus *sn*-2 lysoPS (Lin et al., 2024; Yan et al., 2024; Zhou et al., 2025). In the present work, the striking accumulation of GPR34 KI PC and MemB in the PerC allowed us to probe the PLA1A-lysoPS-GPR34 axis.

Our data suggest that omental stromal cells produce PLA1A, which subsequently generates the bioactive lipid *sn*-2 lysoPS to govern KI cell residence at homeostasis (**Figure 3.1**). This is reminiscent of how omental stromal cells produce chemokine mediators that govern immune cell homing (Ansel et al., 2002; Yoshihara and Okabe, 2023; Perez-Shibayama et al., 2018; Jackson-Jones et al., 2020). However, since lysoPS is not a genetically encoded protein subject to direct transcriptional regulation, it is important to consider both the PLA1A enzyme and its substrate PS. PLA1A has been characterized as a secreted extracellular enzyme, and its distribution and diffusion radius are unknown. Measurable levels of the enzyme in human serum (Zhao et al., 2021) suggest that some fraction of PLA1A may be systemic. Yet local production is likely relevant in the setting of GPR34 KI-mediated PerC immune cell accumulation because KI cells were spatially enriched at the omentum, consistent with the existence of a ligand gradient. Meanwhile, the availability of cell surface PLA1A-accessible PS in the homeostatic omentum is unclear. Although externalized PS might derive from basal levels of apoptosis (Hosono et al.,

2001), transiently exposed PS on live cell membranes could also be the relevant source (Zhao et al., 2021; Segawa et al., 2011; Elliott et al., 2005). Since GPR34 structures indicate that lysoPS enters the ligand-binding pocket laterally from within the lipid bilayer (Xia et al., 2023; Liu et al., 2023; Izume et al., 2024), any *sn*-2 lysoPS molecule that activates the receptor presumably first positions itself in the outer leaflet of the GPR34-expressing cell's plasma membrane. This could happen either if a PS molecule were externalized on the GPR34-expressing cell's surface or if *sn*-2 lysoPS were transferred from another cell. Lipid transfer between cells can occur via exosome trafficking (Wang et al., 2020) and trogocytosis (Aucher et al., 2008).

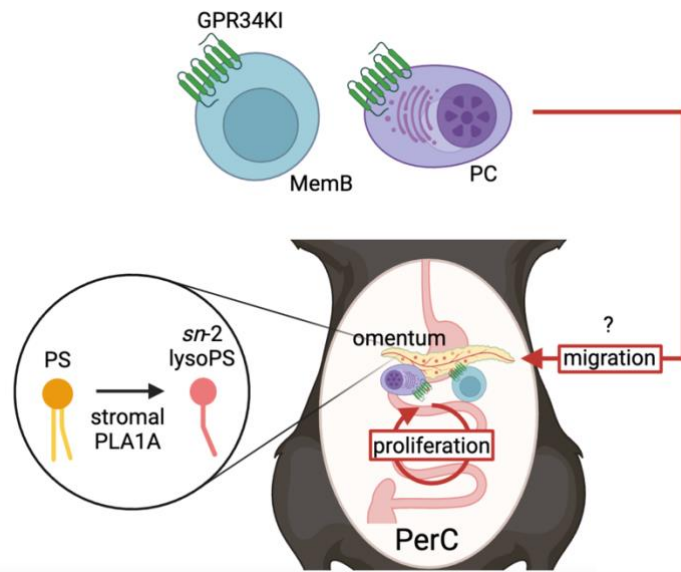


**Figure 3.1. Model for GPR34 KI PerC PC and MemB accumulation.**

Stromal PLA1A produces *sn*-2 lysoPS at the omentum, which is required for the local accumulation of GPR34 KI PC and MemB. GPR34KI promotes the proliferation of PerC MemB and mediates the ex vivo migration of B-lineage lymphocytes.

On the receptor front, this work showed that GPR34 KI can promote cell proliferation in vivo and that GPR34-mediated cell cycle activation occurs in a cell-type specific manner. PerC KI MemB divided more than their WT counterparts, while PC, B1 cells, and B2 cells did not,

suggesting a requirement for a synergistic cell state. These findings add nuance to prior in vitro studies where transfection of GPR34 into cell lines uniformly led to pro-growth signaling (Sugo et al., 2006; Ansell et al., 2012; Korona et al., 2021). In contrast to the PLA1A-dependent accumulation of PerC KI MemB, their proliferative advantage was PLA1A-independent. This result indicates that KI MemB abundance in the PerC cannot be attributed solely to cell division. Furthermore, there are likely two modes of GPR34 KI signaling—one mediating accumulation through *sn*-2 lysoPS, and one mediating proliferation through either constitutive activity or PLA1A-independent ligands such as *sn*-1 lysoPS.

Transwell migration assays demonstrated that GPR34 KI promotes ex vivo migration, but intravenous adoptive transfer experiments failed to establish whether KI cells home to the PerC in vivo. Technical challenges, including limited donor cell numbers and ex vivo plasma cell fragility (Nguyen et al., 2018), could have limited our ability to detect trafficking from the blood. Alternatively, the assumption that KI cells arrive in the PerC via the circulation could be incorrect. PerC immune cells canonically migrate to the PerC via omental capillaries within FALCs (Ansel et al., 2002; Jackson-Jones and Bénézech, 2020), but we are open to the possibility that GPR34 KI cells take a non-hematogenous route such as through lymphatics or across the visceral peritoneal linings of PerC organs. Nevertheless, given the virtual absence of PC in the PerC of WT mice, it seems likely that the accumulation of KI PC involves at least some level of cell recruitment. Based on the depletion of reporter positive KI PC from the gut and on the IgA<sup>+</sup>CCR9<sup>+</sup> profile of PerC KI PC, we speculate that KI PC are generated in the PP and diverted to the PerC instead of homing to the intestinal LP. However, we cannot exclude the possibility that some KI PC differentiate locally from MemB or the possibility that the KI receptor causes retention of PC that are already in the PerC.

Despite our original goal of modeling GPR34 GOF-driven malignancy, KI mice did not develop SG KI cell accumulation or lymphoma. In humans, SG MALT lymphoma arises in a Sjogren's syndrome context of chronic autoimmunity (Korona et al., 2021; Pringle et al., 2022). Thus, we propose that future attempts to study GPR34's role in lymphoma should be performed in mouse models of Sjogren's syndrome that recapitulate both immune cell SG infiltration and epithelial cell apoptosis (Gao et al., 2020). While homeostatic levels of PS and PLA1A yield sufficient *sn*-2 lysoPS for KI cell accumulation in the PerC, outgrowth of GPR34 GOF-harboring tumor cells in the SG may require higher lysoPS levels, achieved only when PLA1A has access to abundant apoptotic PS substrate. Moreover, GPR34 likely cooperates with other factors to promote KI cell localization in the PerC, and these factors may be absent in the uninfamed SG.

In conclusion, we demonstrate that PLA1A produces *sn*-2 lysoPS that can regulate GPR34-mediated immune cell localization in the PerC. This work establishes the first in vivo link between GPR34 and PLA1A and adds to our understanding of the chemoattractant systems that direct immune cell trafficking to body cavities. In the future, the GPR34 GOF KI mouse model may be useful not only for further studies of GPR34-driven lymphoma but also for overexpression of the receptor by any cell type of interest. We speculate that the PLA1A-lysoPS-GPR34 axis will be relevant in additional immune contexts.

## REFERENCES

- Akasaka, T., Y.-F. Lee, A.J. Novak, G. Honjo, K. Takeoka, F. Maekawa, K. Fukutsuka, M. Hayashida, and H. Ohno. 2017. Clinical, histopathological, and molecular features of mucosa-associated lymphoid tissue (MALT) lymphoma carrying the t(X;14)(p11;q32)/GPR34-immunoglobulin heavy chain gene. *Leukemia & Lymphoma*. 58:2247–2250. doi:10.1080/10428194.2017.1289525.
- Ansel, K.M., R.B.S. Harris, and J.G. Cyster. 2002. CXCL13 Is Required for B1 Cell Homing, Natural Antibody Production, and Body Cavity Immunity. *Immunity*. 16:67–76. doi:10.1016/S1074-7613(01)00257-6.
- Ansell, S.M., T. Akasaka, E. McPhail, M. Manske, E. Braggio, T. Price-Troska, S. Ziesmer, F. Secreto, R. Fonseca, M. Gupta, M. Law, T.E. Witzig, M.J.S. Dyer, A. Dogan, J.R. Cerhan, and A.J. Novak. 2012. t(X;14)(p11;q32) in MALT lymphoma involving GPR34 reveals a role for GPR34 in tumor cell growth. *Blood*. 120:3949–3957. doi:10.1182/blood-2011-11-389908.
- Aoki, J., Y. Nagai, H. Hosono, K. Inoue, and H. Arai. 2002. Structure and function of phosphatidylserine-specific phospholipase A1. *Biochimica et Biophysica Acta (BBA) - Molecular and Cell Biology of Lipids*. 1582:26–32. doi:10.1016/S1388-1981(02)00134-8.
- Aucher, A., E. Magdeleine, E. Joly, and D. Hudrisier. 2008. Capture of plasma membrane fragments from target cells by trogocytosis requires signaling in T cells but not in B cells. *Blood*. 111:5621–5628. doi:10.1182/blood-2008-01-134155.
- van Baal, J.O.A.M., K.K. Van de Vijver, R. Nieuwland, C.J.F. van Noorden, W.J. van Driel, A. Sturk, G.G. Kenter, L.G. Rikkert, and C.A.R. Lok. 2017. The histophysiology and

- pathophysiology of the peritoneum. *Tissue and Cell*. 49:95–105.  
doi:10.1016/j.tice.2016.11.004.
- Baens, M., J.F. Ferreiro, T. Tousseyn, H. Urbankova, L. Michaux, L. de Leval, D. Dierickx, P. Wolter, X. Sagaert, P. Vandenberghe, C.D. Wolf-Peeters, and I. Wlodarska. 2012. t(X;14)(p11.4;q32.33) is recurrent in marginal zone lymphoma and up-regulates GPR34. *1*. 97:184–188. doi:10.3324/haematol.2011.052639.
- Bella, Á., C.A. Di Trani, M. Fernández-Sendin, L. Arrizabalaga, A. Cirella, Á. Teijeira, J. Medina-Echeverz, I. Melero, P. Berraondo, and F. Aranda. 2021. Mouse Models of Peritoneal Carcinomatosis to Develop Clinical Applications. *Cancers*. 13:963.  
doi:10.3390/cancers13050963.
- Bénézech, C., N.-T. Luu, J.A. Walker, A.A. Kruglov, Y. Loo, K. Nakamura, Y. Zhang, S. Nayar, L.H. Jones, A. Flores-Langarica, A. McIntosh, J. Marshall, F. Barone, G. Besra, K. Miles, J.E. Allen, M. Gray, G. Kollias, A.F. Cunningham, D.R. Withers, K.M. Toellner, N.D. Jones, M. Veldhoen, S.A. Nedospasov, A.N.J. McKenzie, and J.H. Caamaño. 2015. Inflammation-induced formation of fat-associated lymphoid clusters. *Nat Immunol*. 16:819–828. doi:10.1038/ni.3215.
- Bhattacharya, D., M.T. Cheah, C.B. Franco, N. Hosen, C.L. Pin, W.C. Sha, and I.L. Weissman. 2007. Transcriptional profiling of antigen-dependent murine B cell differentiation and memory formation. *J Immunol*. 179:6808–6819. doi:10.4049/jimmunol.179.10.6808.
- Blankman, J.L., J.Z. Long, S.A. Trauger, G. Siuzdak, and B.F. Cravatt. 2013. ABHD12 controls brain lysophosphatidylserine pathways that are deregulated in a murine model of the neurodegenerative disease PHARC. *PNAS*. 110:1500–1505.  
doi:10.1073/pnas.1217121110.

- Campbell, S.M., J.A. Knipper, D. Ruckerl, C.M. Finlay, N. Logan, C.M. Minutti, M. Mack, S.J. Jenkins, M.D. Taylor, and J.E. Allen. Myeloid cell recruitment versus local proliferation differentiates susceptibility from resistance to filarial infection. *eLife*. 7:e30947. doi:10.7554/eLife.30947.
- Cerutti, A., M. Cols, and I. Puga. 2013. Marginal zone B cells: virtues of innate-like antibody-producing lymphocytes. *Nat Rev Immunol*. 13:118–132. doi:10.1038/nri3383.
- Chakraborty, A., and S.S. Kamat. 2024. Lysophosphatidylserine: A Signaling Lipid with Implications in Human Diseases. *Chem. Rev*. 124:5470–5504. doi:10.1021/acs.chemrev.3c00701.
- Chakraborty, A., P. Punnamraju, T. Sajeevan, A. Kaur, U. Kolthur-Seetharam, and S.S. Kamat. 2025. Identification of ABHD6 as a lysophosphatidylserine lipase in the mammalian liver and kidneys. *Journal of Biological Chemistry*. 108157. doi:10.1016/j.jbc.2025.108157.
- Chang, W., H. Fa, D. Xiao, and J. Wang. 2020. Targeting phosphatidylserine for Cancer therapy: prospects and challenges. *Theranostics*. 10:9214–9229. doi:10.7150/thno.45125.
- Christian, D.A., T.A. Adams, L.A. Shallberg, A.T. Phan, T.E. Smith, M. Abraha, J. Perry, G. Ruthel, J.T. Clark, G.H. Pritchard, L.R. Aronson, S. Gossa, D.B. McGavern, R.M. Kedl, and C.A. Hunter. 2022. cDC1 coordinate innate and adaptive responses in the omentum required for T cell priming and memory. *Sci. Immunol*. 7:eabq7432. doi:10.1126/sciimmunol.abq7432.
- Clements, T.W., M. Tolonen, C.G. Ball, and A.W. Kirkpatrick. 2021. Secondary Peritonitis and Intra-Abdominal Sepsis: An Increasingly Global Disease in Search of Better Systemic Therapies. *Scand J Surg*. 110:139–149. doi:10.1177/1457496920984078.
- Cocolini, F. 2013. Peritoneal carcinomatosis. *WJG*. 19:6979. doi:10.3748/wjg.v19.i41.6979.

- Cortés-Guiral, D., M. Hübner, M. Alyami, A. Bhatt, W. Ceelen, O. Glehen, F. Lordick, R. Ramsay, O. Sgarbura, K. Van Der Speeten, K.K. Turaga, and M. Chand. 2021. Primary and metastatic peritoneal surface malignancies. *Nat Rev Dis Primers*. 7:91. doi:10.1038/s41572-021-00326-6.
- Cruz-Migoni, S., and J. Caamaño. 2016. Fat-Associated Lymphoid Clusters in Inflammation and Immunity. *Front. Immunol*. 7. doi:10.3389/fimmu.2016.00612.
- De Giovanni, M., H. Tam, C. Valet, Y. Xu, M.R. Looney, and J.G. Cyster. 2022. GPR35 promotes neutrophil recruitment in response to serotonin metabolite 5-HIAA. *Cell*. 185:815-830.e19. doi:10.1016/j.cell.2022.01.010.
- Duan, L., D. Liu, H. Chen, M.A. Mintz, M.Y. Chou, D.I. Kotov, Y. Xu, J. An, B.J. Laidlaw, and J.G. Cyster. 2021. Follicular dendritic cells restrict interleukin-4 availability in germinal centers and foster memory B cell generation. *Immunity*. 54:2256-2272.e6. doi:10.1016/j.immuni.2021.08.028.
- Elliott, J.I., A. Surprenant, F.M. Marelli-Berg, J.C. Cooper, R.L. Cassady-Cain, C. Wooding, K. Linton, D.R. Alexander, and C.F. Higgins. 2005. Membrane phosphatidylserine distribution as a non-apoptotic signalling mechanism in lymphocytes. *Nat Cell Biol*. 7:808–816. doi:10.1038/ncb1279.
- Etzerodt, A., M. Moulin, T.K. Doktor, M. Delfini, N. Mossadegh-Keller, M. Bajenoff, M.H. Sieweke, S.K. Moestrup, N. Auphan-Anezin, and T. Lawrence. 2020. Tissue-resident macrophages in omentum promote metastatic spread of ovarian cancer. *J Exp Med*. 217:e20191869. doi:10.1084/jem.20191869.
- Flies, D.B., T. Higuchi, J.C. Harris, V. Jha, P.A. Gimotty, and S.F. Adams. 2016. Immune checkpoint blockade reveals the stimulatory capacity of tumor-associated CD103<sup>+</sup>

- dendritic cells in late-stage ovarian cancer. *OncoImmunology*. 5:e1185583.  
doi:10.1080/2162402X.2016.1185583.
- Gao, Y., Y. Chen, Z. Zhang, X. Yu, and J. Zheng. 2020. Recent Advances in Mouse Models of Sjögren's Syndrome. *Front Immunol*. 11:1158. doi:10.3389/fimmu.2020.01158.
- Haro, M.A., A.M. Dyevoich, J.P. Phipps, and K.M. Haas. 2019. Activation of B-1 Cells Promotes Tumor Cell Killing in the Peritoneal Cavity. *Cancer Research*. 79:159–170.  
doi:10.1158/0008-5472.CAN-18-0981.
- Hosono, H., J. Aoki, Y. Nagai, K. Bandoh, M. Ishida, R. Taguchi, H. Arai, and K. Inoue. 2001. Phosphatidylserine-specific Phospholipase A1 Stimulates Histamine Release from Rat Peritoneal Mast Cells through Production of 2-Acyl-1-lysophosphatidylserine\*. *Journal of Biological Chemistry*. 276:29664–29670. doi:10.1074/jbc.M104597200.
- Iida, Y., N. H. Tsuno, J. Kishikawa, K. Kaneko, K. Muro, K. Kawai, T. Ikeda, S. Ishihara, H. Yamaguchi, E. Sunami, J. Kitayama, Y. Yatomi, and T. Watanabe. 2014. Lysophosphatidylserine Stimulates Chemotactic Migration of Colorectal Cancer Cells Through GPR34 and PI3K/Akt Pathway. *Anticancer Research*. 34:5465–5472.
- Inoue, A., F. Raimondi, F.M.N. Kadji, G. Singh, T. Kishi, A. Uwamizu, Y. Ono, Y. Shinjo, S. Ishida, N. Arang, K. Kawakami, J.S. Gutkind, J. Aoki, and R.B. Russell. 2019. Illuminating G-Protein-Coupling Selectivity of GPCRs. *Cell*. 177:1933-1947.e25.  
doi:10.1016/j.cell.2019.04.044.
- Isaza-Restrepo, A., J.S. Martin-Saavedra, J.L. Velez-Leal, F. Vargas-Barato, and R. Riveros-Dueñas. 2018. The Peritoneum: Beyond the Tissue – A Review. *Front. Physiol*. 9:738.  
doi:10.3389/fphys.2018.00738.

- Isho, B., A. Florescu, A.A. Wang, and J.L. Gommerman. 2021. Fantastic IgA plasma cells and where to find them. *Immunol Rev.* 303:119–137. doi:10.1111/imr.12980.
- Izume, T., R. Kawahara, A. Uwamizu, L. Chen, S. Yaginuma, J. Omi, H. Kawana, F. Hou, F.K. Sano, T. Tanaka, K. Kobayashi, H.H. Okamoto, Y. Kise, T. Ohwada, J. Aoki, W. Shihoya, and O. Nureki. 2024. Structural basis for lysophosphatidylserine recognition by GPR34. *Nat Commun.* 15:902. doi:10.1038/s41467-024-45046-z.
- Jackson-Jones, L.H., and C. Bénézech. 2020. FALC stromal cells define a unique immunological niche for the surveillance of serous cavities. *Current Opinion in Immunology.* 64:42–49. doi:10.1016/j.coi.2020.03.008.
- Jackson-Jones, L.H., S.M. Duncan, M.S. Magalhaes, S.M. Campbell, R.M. Maizels, H.J. McSorley, J.E. Allen, and C. Bénézech. 2016. Fat-associated lymphoid clusters control local IgM secretion during pleural infection and lung inflammation. *Nat Commun.* 7:12651. doi:10.1038/ncomms12651.
- Jackson-Jones, L.H., P. Smith, J.R. Portman, M.S. Magalhaes, K.J. Mylonas, M.M. Vermeren, M. Nixon, B.E.P. Henderson, R. Dobie, S. Vermeren, L. Denby, N.C. Henderson, D.J. Mole, and C. Bénézech. 2020. Stromal Cells Covering Omental Fat-Associated Lymphoid Clusters Trigger Formation of Neutrophil Aggregates to Capture Peritoneal Contaminants. *Immunity.* 52:700-715.e6. doi:10.1016/j.immuni.2020.03.011.
- Jin, Z.-T., K. Li, M. Li, Z.-G. Ren, F.-S. Wang, J.-Y. Zhu, X.-S. Leng, and W.-D. Yu. 2015. G-protein Coupled Receptor 34 Knockdown Impairs the Proliferation and Migration of HGC-27 Gastric Cancer Cells In Vitro. *Chin Med J (Engl).* 128:545–549. doi:10.4103/0366-6999.151114.

- Joshi, A., M. Shaikh, S. Singh, A. Rajendran, A. Mhetre, and S.S. Kamat. 2018. Biochemical characterization of the PHARC-associated serine hydrolase ABHD12 reveals its preference for very-long-chain lipids. *J Biol Chem.* 293:16953–16963. doi:10.1074/jbc.RA118.005640.
- Kamat, S.S., K. Camara, W.H. Parsons, D.-H. Chen, M.M. Dix, T.D. Bird, A.R. Howell, and B.F. Cravatt. 2015. Immunomodulatory lysophosphatidylserines are regulated by ABHD16A and ABHD12 interplay. *Nat Chem Biol.* 11:164–171. doi:10.1038/nchembio.1721.
- Kim, K.-W., J.W. Williams, Y.-T. Wang, S. Ivanov, S. Gilfillan, M. Colonna, H.W. Virgin, E.L. Gautier, and G.J. Randolph. 2016. MHC II<sup>+</sup> resident peritoneal and pleural macrophages rely on IRF4 for development from circulating monocytes. *J Exp Med.* 213:1951–1959. doi:10.1084/jem.20160486.
- Kitamura, H., K. Makide, A. Shuto, M. Ikubo, A. Inoue, K. Suzuki, Y. Sato, S. Nakamura, Y. Otani, T. Ohwada, and J. Aoki. 2012. GPR34 is a receptor for lysophosphatidylserine with a fatty acid at the sn-2 position. *The Journal of Biochemistry.* 151:511–518. doi:10.1093/jb/mvs011.
- Korona, B., D. Korona, W. Zhao, A. Wotherspoon, and M.-Q. Du. 2021. GPR34 activation potentially bridges lymphoepithelial lesion to genesis of salivary gland MALT lymphoma. *Blood.* doi:10.1182/blood.2020010495.
- Kraus, M., M.B. Alimzhanov, N. Rajewsky, and K. Rajewsky. 2004. Survival of resting mature B lymphocytes depends on BCR signaling via the Igalpha/beta heterodimer. *Cell.* 117:787–800. doi:10.1016/j.cell.2004.05.014.
- Leendertse, M., R.J.L. Willems, I.A.J. Giebelen, J.J.T.H. Roelofs, N. van Rooijen, M.J.M. Bonten, and T. van der Poll. 2009. Peritoneal macrophages are important for the early

- containment of *Enterococcus faecium* peritonitis in mice. *Innate Immun.* 15:3–12.  
doi:10.1177/1753425908100238.
- Lengyel, E., J.E. Burdette, H.A. Kenny, D. Matei, J. Pilrose, P. Haluska, K.P. Nephew, D.B. Hales, and M.S. Stack. 2014. Epithelial ovarian cancer experimental models. *Oncogene.* 33:3619–3633. doi:10.1038/onc.2013.321.
- Leventis, P.A., and S. Grinstein. 2010. The Distribution and Function of Phosphatidylserine in Cellular Membranes. *Annual Review of Biophysics.* 39:407–427.  
doi:10.1146/annurev.biophys.093008.131234.
- Liebscher, I., U. Müller, D. Teupser, E. Engemaier, K.M.Y. Engel, L. Ritscher, D. Thor, K. Sangkuhl, A. Ricken, A. Wurm, D. Piehler, S. Schmutzler, H. Fuhrmann, F.W. Albert, A. Reichenbach, J. Thiery, T. Schöneberg, and A. Schulz. 2011. Altered Immune Response in Mice Deficient for the G Protein-coupled Receptor GPR34\*. *Journal of Biological Chemistry.* 286:2101–2110. doi:10.1074/jbc.M110.196659.
- Lin, B., Y. Zhou, Z. Huang, M. Ma, M. Qi, Z. Jiang, G. Li, Y. Xu, J. Yan, D. Wang, X. Wang, W. Jiang, and R. Zhou. 2024. GPR34 senses demyelination to promote neuroinflammation and pathologies. *Cell Mol Immunol.* 21:1131–1144. doi:10.1038/s41423-024-01204-3.
- Liu, G., X. Li, Y. Wang, X. Zhang, and W. Gong. 2023. Structural basis for ligand recognition and signaling of the lysophosphatidylserine receptors GPR34 and GPR174. *PLoS Biol.* 21:e3002387. doi:10.1371/journal.pbio.3002387.
- Liu, M., A. Silva-Sanchez, T.D. Randall, and S. Meza-Perez. 2021. Specialized immune responses in the peritoneal cavity and omentum. *J Leukoc Biol.* 109:717–729.  
doi:10.1002/JLB.5MIR0720-271RR.

- Lu, E., and J.G. Cyster. 2019. G-protein coupled receptors and ligands that organize humoral immune responses. *Immunol Rev.* 289:158–172. doi:10.1111/imr.12743.
- Makide, K., and J. Aoki. 2013. GPR34 as a lysophosphatidylserine receptor. *The Journal of Biochemistry.* 153:327–329. doi:10.1093/jb/mvt010.
- Martinez-Climent, J.A. 2018. G-protein coupled receptor (GPCR) mutations in lymphoid malignancies: linking immune signaling activation and genetic abnormalities. *Haematologica.* 103:1252–1255. doi:10.3324/haematol.2018.196998.
- Meza-Perez, S., and T.D. Randall. 2017. Immunological Functions of the Omentum. *Trends in Immunology.* 38:526–536. doi:10.1016/j.it.2017.03.002.
- Molina, T.J., P. Lin, S.H. Swerdlow, and J.R. Cook. 2011. Marginal zone lymphomas with plasmacytic differentiation and related disorders. *Am J Clin Pathol.* 136:211–225. doi:10.1309/AJCP63OGXHXCSKSC.
- Moody, S., J.S. Thompson, S.-S. Chuang, H. Liu, M. Raderer, G. Vassiliou, I. Wlodarska, F. Wu, S. Cogliatti, A. Robson, M. Ashton-Key, Y. Bi, J. Goodlad, and M.-Q. Du. 2018. Novel GPR34 and CCR6 mutation and distinct genetic profiles in MALT lymphomas of different sites. *1.* 103:1329–1336. doi:10.3324/haematol.2018.191601.
- Nanduri, J., and J.W. Kazura. 1989. Clinical and Laboratory Aspects of Filariasis. *CLIN. MICROBIOL. REV.* 2.
- Narayanasamy, R., R. Rajasekharan, and D. Usharani. 2023. Molecular insights on PS-PLA1 lipase activity of human ABHD16B. *Biophysical Chemistry.* 296:106976. doi:10.1016/j.bpc.2023.106976.

- Newell, K.L., J. Cox, A.T. Waickman, J.R. Wilmore, and G.M. Winslow. 2022. T-bet<sup>+</sup> B cells Dominate the Peritoneal Cavity B Cell Response during Murine Intracellular Bacterial Infection. *The Journal of Immunology*. 208:2749–2760. doi:10.4049/jimmunol.2101209.
- Nguyen, D.C., S. Garimalla, H. Xiao, S. Kyu, I. Albizua, J. Galipeau, K.-Y. Chiang, E.K. Waller, R. Wu, G. Gibson, J. Roberson, F.E. Lund, T.D. Randall, I. Sanz, and F.E.-H. Lee. 2018. Factors of the bone marrow microniche that support human plasma cell survival and immunoglobulin secretion. *Nat Commun*. 9:3698. doi:10.1038/s41467-018-05853-7.
- Okabe, Y. 2024. Development and organization of omental milky spots. *Immunological Reviews*. 324:68–77. doi:10.1111/imr.13337.
- Okabe, Y., and R. Medzhitov. 2014. Tissue-Specific Signals Control Reversible Program of Localization and Functional Polarization of Macrophages. *Cell*. 157:832–844. doi:10.1016/j.cell.2014.04.016.
- Okudaira, M., A. Inoue, A. Shuto, K. Nakanaga, K. Kano, K. Makide, D. Saigusa, Y. Tomioka, and J. Aoki. 2014. Separation and quantification of 2-acyl-1-lysophospholipids and 1-acyl-2-lysophospholipids in biological samples by LC-MS/MS. *Journal of Lipid Research*. 55:2178–2192. doi:10.1194/jlr.D048439.
- Omi, J., K. Kano, and J. Aoki. 2021. Current Knowledge on the Biology of Lysophosphatidylserine as an Emerging Bioactive Lipid. *Cell Biochem Biophys*. 79:497–508. doi:10.1007/s12013-021-00988-9.
- Oosterling, S.J., G.J. van der Bij, M. Bögels, J.R.M. van der Sijp, R.H.J. Beelen, S. Meijer, and M. van Egmond. 2006. Insufficient ability of omental milky spots to prevent peritoneal tumor outgrowth supports omentectomy in minimal residual disease. *Cancer Immunol Immunother*. 55:1043–1051. doi:10.1007/s00262-005-0101-y.

- Pabst, O., L. Ohl, M. Wendland, M.-A. Wurbel, E. Kremmer, B. Malissen, and R. Förster. 2004. Chemokine receptor CCR9 contributes to the localization of plasma cells to the small intestine. *J Exp Med.* 199:411–416. doi:10.1084/jem.20030996.
- Palm, A.-K.E., and S. Kleinau. 2021. Marginal zone B cells: From housekeeping function to autoimmunity? *J Autoimmun.* 119:102627. doi:10.1016/j.jaut.2021.102627.
- Peison, B., B. Benisch, M.C. Williams, and R. Newman. 1980. Primary extramedullary plasmacytoma of the omentum associated with recurrent adenocarcinoma of the colon: first case report. *Hum Pathol.* 11:399–401. doi:10.1016/s0046-8177(80)80040-2.
- Perez-Shibayama, C., C. Gil-Cruz, H.-W. Cheng, L. Onder, A. Printz, U. Mörbe, M. Novkovic, C. Li, C. Lopez-Macias, M.B. Buechler, S.J. Turley, M. Mack, C. Sonesson, M.D. Robinson, E. Scandella, J. Gommerman, and B. Ludewig. 2018. Fibroblastic reticular cells initiate immune responses in visceral adipose tissues and secure peritoneal immunity. *Sci. Immunol.* 3:eaar4539. doi:10.1126/sciimmunol.aar4539.
- Pietrzak, D., J.W. Łuczak, and M. Wiśniewski. 2024. Beyond Tradition: Exploring Cutting-Edge Approaches for Accurate Diagnosis of Human Filariasis. *Pathogens.* 13:447. doi:10.3390/pathogens13060447.
- Preissler, J., A. Grosche, V. Lede, D.L. Duc, K. Krügel, V. Matyash, F. Szulzewsky, S. Kallendrusch, K. Immig, H. Kettenmann, I. Bechmann, T. Schöneberg, and A. Schulz. 2015. Altered microglial phagocytosis in GPR34-deficient mice. *Glia.* 63:206–215. doi:https://doi.org/10.1002/glia.22744.
- Pringle, S., G.M. Verstappen, M.S. van Ginkel, U. Nakshbandi, Z. Girigoria, H. Bootsma, B. van der Vegt, and F.G.M. Kroese. 2022. Lymphoepithelial lesions in the salivary glands of

- primary Sjögren's syndrome patients: the perfect storm? *Clin Exp Rheumatol*. 40:2434–2442. doi:10.55563/clinexprheumatol/06an99.
- Rajan, B., T. Ramalingam, and T.V. Rajan. 2005. Critical Role for IgM in Host Protection in Experimental Filarial Infection. *The Journal of Immunology*. 175:1827–1833. doi:10.4049/jimmunol.175.3.1827.
- Rangel-Moreno, J., J.E. Moyron-Quiroz, D.M. Carragher, K. Kusser, L. Hartson, A. Moquin, and T.D. Randall. 2009. Omental Milky Spots Develop in the Absence of Lymphoid Tissue-Inducer Cells and Support B and T Cell Responses to Peritoneal Antigens. *Immunity*. 30:731–743. doi:10.1016/j.immuni.2009.03.014.
- Rei, M., N. Gonçalves-Sousa, T. Lança, R.G. Thompson, S. Mensurado, F.R. Balkwill, H. Kulbe, D.J. Pennington, and B. Silva-Santos. 2014. Murine CD27(-) V $\gamma$ 6(+)  $\gamma\delta$  T cells producing IL-17A promote ovarian cancer growth via mobilization of protumor small peritoneal macrophages. *Proc Natl Acad Sci U S A*. 111:E3562-3570. doi:10.1073/pnas.1403424111.
- Ritter, M., W.P.C. Ndongmo, A.J. Njouendou, N.N. Nghochuzie, L.C. Nchang, D.B. Tayong, K. Arndts, N. Nausch, M. Jacobsen, S. Wanji, L.E. Layland, and A. Hoerauf. 2018. *Mansonella perstans* microfilaremic individuals are characterized by enhanced type 2 helper T and regulatory T and B cell subsets and dampened systemic innate and adaptive immune responses. *PLoS Negl Trop Dis*. 12:e0006184. doi:10.1371/journal.pntd.0006184.
- Robinson, M.J., Z. Ding, M.R. Dowling, D.L. Hill, R.H. Webster, C. McKenzie, C. Pitt, K. O'Donnell, J. Mulder, E. Brodie, P.D. Hodgkin, N.C. Wong, I. Quast, and D.M. Tarlinton. 2023. Intrinsically determined turnover underlies broad heterogeneity in plasma-cell lifespan. *Immunity*. 56:1596-1612.e4. doi:10.1016/j.immuni.2023.04.015.

- Ross, J.T., M.A. Matthay, and H.W. Harris. 2018. Secondary peritonitis: principles of diagnosis and intervention. *BMJ*. 361:k1407. doi:10.1136/bmj.k1407.
- Roy, B., A.-M. Brennecke, S. Agarwal, M. Krey, S. Düber, and S. Weiss. 2013. An Intrinsic Propensity of Murine Peritoneal B1b Cells to Switch to IgA in Presence of TGF- $\beta$  and Retinoic Acid. *PLoS One*. 8:e82121. doi:10.1371/journal.pone.0082121.
- Sayo, A., H. Konishi, M. Kobayashi, K. Kano, H. Kobayashi, H. Hibi, J. Aoki, and H. Kiyama. 2019. GPR34 in spinal microglia exacerbates neuropathic pain in mice. *Journal of Neuroinflammation*. 16:82. doi:10.1186/s12974-019-1458-8.
- Schöneberg, T., J. Meister, A.B. Knierim, and A. Schulz. 2018. The G protein-coupled receptor GPR34 – The past 20 years of a grownup. *Pharmacology & Therapeutics*. 189:71–88. doi:10.1016/j.pharmthera.2018.04.008.
- Segawa, K., J. Suzuki, and S. Nagata. 2011. Constitutive exposure of phosphatidylserine on viable cells. *Proc Natl Acad Sci U S A*. 108:19246–19251. doi:10.1073/pnas.1114799108.
- Singh, S., A. Joshi, and S.S. Kamat. 2020. Mapping the Neuroanatomy of ABHD16A, ABHD12, and Lysophosphatidylserines Provides New Insights into the Pathophysiology of the Human Neurological Disorder PHARC. *Biochemistry*. 59:2299–2311. doi:10.1021/acs.biochem.0c00349.
- Smith, K.G., A. Light, L.A. O'Reilly, S.M. Ang, A. Strasser, and D. Tarlinton. 2000. bcl-2 transgene expression inhibits apoptosis in the germinal center and reveals differences in the selection of memory B cells and bone marrow antibody-forming cells. *J Exp Med*. 191:475–484. doi:10.1084/jem.191.3.475.

- Smith, K.G., U. Weiss, K. Rajewsky, G.J. Nossal, and D.M. Tarlinton. 1994. Bcl-2 increases memory B cell recruitment but does not perturb selection in germinal centers. *Immunity*. 1:803–813. doi:10.1016/s1074-7613(94)80022-7.
- Soliman, K., J. Herberth, T. Fülöp, A. Duong, and R.L. Sturdivant. 2019. Refractory ascites as a presenting feature of extramedullary plasmacytoma in an end-stage renal disease patient with HIV infection. *Clin Nephrol Case Stud*. 7:7–10. doi:10.5414/CNCS109560.
- Song, J., C. Wu, X. Zhang, and L.M. Sorokin. 2013. In Vivo Processing of CXCL5 (LIX) by Matrix Metalloproteinase (MMP)-2 and MMP-9 Promotes Early Neutrophil Recruitment in IL-1 $\beta$ -Induced Peritonitis. *J.I.* 190:401–410. doi:10.4049/jimmunol.1202286.
- Sorensen, E.W., S.A. Gerber, A.L. Sedlacek, V.Y. Rybalko, W.M. Chan, and E.M. Lord. 2009. Omental immune aggregates and tumor metastasis within the peritoneal cavity. *Immunol Res*. 45:185–194. doi:10.1007/s12026-009-8100-2.
- Strasser, A., S. Whittingham, D.L. Vaux, M.L. Bath, J.M. Adams, S. Cory, and A.W. Harris. 1991. Enforced BCL2 expression in B-lymphoid cells prolongs antibody responses and elicits autoimmune disease. *Proc Natl Acad Sci U S A*. 88:8661–8665. doi:10.1073/pnas.88.19.8661.
- Sugo, T., H. Tachimoto, T. Chikatsu, Y. Murakami, Y. Kikukawa, S. Sato, K. Kikuchi, T. Nagi, M. Harada, K. Ogi, M. Ebisawa, and M. Mori. 2006. Identification of a lysophosphatidylserine receptor on mast cells. *Biochemical and Biophysical Research Communications*. 341:1078–1087. doi:10.1016/j.bbrc.2006.01.069.
- Ta-Tang, T.-H., J.L. Crainey, R.J. Post, S.L. Luz, and J.M. Rubio. 2018. Mansonellosis: current perspectives. *Res Rep Trop Med*. 9:9–24. doi:10.2147/RRTM.S125750.

- Thambi, S.M., S.G. Nair, and R. Benson. 2018. Plasmacytoma of the mesentery. *J Postgrad Med.* 64:255–257. doi:10.4103/jpgm.JPGM\_296\_18.
- Thomas, G., J.L. Betters, C.C. Lord, A.L. Brown, S. Marshall, D. Ferguson, J. Sawyer, M.A. Davis, J.T. Melchior, L.C. Blume, A.C. Howlett, P.T. Ivanova, S.B. Milne, D.S. Myers, I. Mrak, V. Leber, C. Heier, U. Taschler, J.L. Blankman, B.F. Cravatt, R.G. Lee, R.M. Crooke, M.J. Graham, R. Zimmermann, H.A. Brown, and J.M. Brown. 2013. The Serine Hydrolase ABHD6 is a Critical Regulator of the Metabolic Syndrome. *Cell Rep.* 5:10.1016/j.celrep.2013.08.047. doi:10.1016/j.celrep.2013.08.047.
- Troppan, K., K. Wenzl, P. Neumeister, and A. Deutsch. 2015. Molecular Pathogenesis of MALT Lymphoma. *Gastroenterol Res Pract.* 2015:102656. doi:10.1155/2015/102656.
- Uwamizu, A., A. Inoue, K. Suzuki, M. Okudaira, A. Shuto, Y. Shinjo, J. Ishiguro, K. Makide, M. Ikubo, S. Nakamura, S. Jung, M. Sayama, Y. Otani, T. Ohwada, and J. Aoki. 2015. Lysophosphatidylserine analogues differentially activate three LysoPS receptors. *The Journal of Biochemistry.* 157:151–160. doi:10.1093/jb/mvu060.
- Uzunköy, A., H. Ozbilge, and M. Horoz. 2009. The influence of omentectomy on bacterial clearance: an experimental study. *Ulus Travma Acil Cerrahi Derg.* 15:541–545.
- Vega-Pérez, A., L.H. Villarrubia, C. Godio, A. Gutiérrez-González, L. Feo-Lucas, M. Ferriz, N. Martínez-Puente, J. Alcaín, A. Mora, G. Sabio, M. López-Bravo, and C. Ardavín. 2021. Resident macrophage-dependent immune cell scaffolds drive anti-bacterial defense in the peritoneal cavity. *Immunity.* 54:2578-2594.e5. doi:10.1016/j.immuni.2021.10.007.
- Wang, A.W., D.M. Cauvi, D. Hawisher, T. Reyes, R. Coimbra, S. Bickler, and A. De Maio. 2019. The Contribution of the Omentum to the Outcome From Sepsis: An Experimental Animal Study. *Shock.* 52:604. doi:10.1097/SHK.0000000000001311.

- Wang, W., N. Zhu, T. Yan, Y.-N. Shi, J. Chen, C.-J. Zhang, X.-J. Xie, D.-F. Liao, and L. Qin. 2020. The crosstalk: exosomes and lipid metabolism. *Cell Communication and Signaling*. 18:119. doi:10.1186/s12964-020-00581-2.
- Wang, X., J. Cai, B. Lin, M. Ma, Y. Tao, Y. Zhou, L. Bai, W. Jiang, and R. Zhou. 2021. GPR34-mediated sensing of lysophosphatidylserine released by apoptotic neutrophils activates type 3 innate lymphoid cells to mediate tissue repair. *Immunity*. 54:1123-1136.e8. doi:10.1016/j.immuni.2021.05.007.
- Wöhrrer, S., M. Troch, B. Streubel, M. Hoffmann, L. Müllauer, A. Chott, and M. Raderer. 2007. Pathology and clinical course of MALT lymphoma with plasmacytic differentiation. *Ann Oncol*. 18:2020–2024. doi:10.1093/annonc/mdm375.
- Xia, A., X. Yong, C. Zhang, G. Lin, G. Jia, C. Zhao, X. Wang, Y. Hao, Y. Wang, P. Zhou, X. Yang, Y. Deng, C. Wu, Y. Chen, J. Zhu, X. Tang, J. Liu, S. Zhang, J. Zhang, Z. Xu, Q. Hu, J. Zhao, Y. Yue, W. Yan, Z. Su, Y. Wei, R. Zhou, H. Dong, Z. Shao, and S. Yang. 2023. Cryo-EM structures of human GPR34 enable the identification of selective antagonists. *Proc Natl Acad Sci U S A*. 120:e2308435120. doi:10.1073/pnas.2308435120.
- Yan, J., C. Zhang, Y. Xu, Z. Huang, Q. Ye, X. Qian, L. Zhu, G. Huang, X. Wang, W. Jiang, and R. Zhou. 2024. GPR34 is a metabolic immune checkpoint for ILC1-mediated antitumor immunity. *Nat Immunol*. 25:2057–2067. doi:10.1038/s41590-024-01973-z.
- Yang, P., Q. Liu, H. Zhang, M. Wu, J. Zhao, G. Shen, and Y. Zhao. 2025. Risk relationship between six autoimmune diseases and malignancies: An umbrella review. *Autoimmun Rev*. 24:103779. doi:10.1016/j.autrev.2025.103779.

- Yang, Z., and C.D.C. Allen. 2018. Expression of Exogenous Genes in Murine Primary B Cells and B Cell Lines Using Retroviral Vectors. *Methods Mol Biol.* 1707:39–49.  
doi:10.1007/978-1-4939-7474-0\_3.
- Yordanova, I.A., K. Jürchott, S. Steinfeldler, K. Vogt, U. Krüger, A.A. Köhl, B. Sawitzki, and S. Hartmann. 2022. The Host Peritoneal Cavity Harbors Prominent Memory Th2 and Early Recall Responses to an Intestinal Nematode. *Front. Immunol.* 13:842870.  
doi:10.3389/fimmu.2022.842870.
- Yoshihara, T., and Y. Okabe. 2023. Aldh1a2<sup>+</sup> fibroblastic reticular cells regulate lymphocyte recruitment in omental milky spots. *J Exp Med.* 220:e20221813.  
doi:10.1084/jem.20221813.
- Zhao, Y., F. Aoudjit, and S.G. Bourgoïn. 2022. Phospholipase A1 Member A Deficiency Alleviates Mannan-Induced Psoriatic Arthritis in Mice Model. *IJMS.* 23:8559.  
doi:10.3390/ijms23158559.
- Zhao, Y., S. Hasse, and S.G. Bourgoïn. 2021. Phosphatidylserine-specific phospholipase A1: A friend or the devil in disguise. *Progress in Lipid Research.* 83:101112.  
doi:10.1016/j.plipres.2021.101112.
- Zhou, Y., M. Chang, N. Wang, Y. Zhuang, F. Wang, X. Zhang, M. Guo, N. Lin, J.Z. Li, and Q. Wang. 2022. Phosphatidylserine-Specific Phospholipase A1 Limits Aggressiveness of Lung Adenocarcinoma by Lysophosphatidylserine and Protein Kinase A–Dependent Pathway. *The American Journal of Pathology.* 192:970–983.  
doi:10.1016/j.ajpath.2022.03.005.
- Zhou, Y., Z. Huang, B. Lin, M. Ma, Y. Hao, J. Liu, W. Xu, G. Huang, W. Mo, X. Wang, W. Jiang, and R. Zhou. 2025. Demyelination-derived lysophosphatidylserine promotes microglial

dysfunction and neuropathology in a mouse model of Alzheimer's disease. *Cell Mol Immunol.* 1–16. doi:10.1038/s41423-024-01235-w.

## Publishing Agreement

It is the policy of the University to encourage open access and broad distribution of all theses, dissertations, and manuscripts. The Graduate Division will facilitate the distribution of UCSF theses, dissertations, and manuscripts to the UCSF Library for open access and distribution. UCSF will make such theses, dissertations, and manuscripts accessible to the public and will take reasonable steps to preserve these works in perpetuity.

I hereby grant the non-exclusive, perpetual right to The Regents of the University of California to reproduce, publicly display, distribute, preserve, and publish copies of my thesis, dissertation, or manuscript in any form or media, now existing or later derived, including access online for teaching, research, and public service purposes.

DocuSigned by:

*Hanson Tam*

6EA3DA8F1394442...

\_\_\_\_\_  
Author Signature

3/12/2025

\_\_\_\_\_  
Date